SOLUTION METHODOLOGY FOR CONSTRAINED EIGENVALUE PROBLEMS AND ITS APPLICATIONS WITH EXPERIMENTAL VALIDATION IN STRUCTURAL CHARACTERISTICS IDENTIFICATION

by

LONGHAN CHEN

A dissertation submitted in partial fulfillment of the
requirements for the degree of

MECHANICAL ENGINEERING

2021

Oakland University
Rochester, Michigan

Doctoral Advisory Committee:

Randy J. Gu, Ph.D., Chair
Lianxiang Yang, Ph.D.
Zissimos P. Mourelatos, Ph.D.
Anna Spagnuolo, Ph.D.

To my mother Yanping Hu, father Fuen Chen, my wife Xiangzhe Ye and my mother-in-law Yunhong Yang

ACKNOWLEDGMENTS

I would like to deeply thank my PhD advisors, Professor Randy J. Gu, not only for excellent academic advice, but also for all kinds of support over the past five years. Professor Gu is the funniest advisor and one of the smartest people I know. He has been supportive and provided insightful discussions about the research.

I am also very grateful to Professor Yang for his scientific advice and knowledge and many insightful discussions and suggestions. I also have to thank the members of my PhD committee, Professor Mourelatos and Professor Spagnuolo, for their helpful career advice and suggestions in general.

Finally, I want to give my best regards to Dr. Qian Zou, Dr. Gary Barber, Dr. Rui Zhu, Dr. Jian Zhu, Mr. Rui Li, Mr. Xinyun Wang, Mr. Dongfu Han and all those who gave me help and support in my graduate studies.

Longhan Chen

ABSTRACT

SOLUTION METHODOLOGY FOR CONSTRAINED EIGENVALUE PROBLEMS AND ITS APPLICATIONS WITH EXPERIMENTAL VALIDATION IN STRUCTURAL CHARACTERISTICS IDENTIFICATION

by

LONGHAN CHEN

Adviser: Randy J.Gu, Ph.D.

A numerical reverse algorithm was developed in this dissertation to find some unknown parameters of an object. For example, if the natural frequency of an object is known, find the mass of the particle placed at a specific place in the object. There is no such direct formula or algorithm that can solve this kind of problem, we can use the reverse algorithm to solve it. Since the objective function can be built after the structure's stiffness matrix and mass matrix were obtained using the finite element method, and the structure's natural frequencies are known, this kind of problem becomes a constrained eigenvalue problem. The constrained eigenvalue problem can be solved by minimizing the objective function and executed using numerical methods. In this dissertation, we developed Newton's iteration to solve it and also developed the Genetic Algorithm as an alternative algorithm when Newton's iteration cannot find unknown parameters. Several numerical examples, such as beam, plane frame, three-dimensional frame, and plate structure, were chosen to test the proposed algorithm's feasibility, accuracy, and solving time. Furthermore, some groups of experimental validation were also provided to testify to it.

TABLE OF CONTENTS

TABLE OF CONTENTS—Continued

LIST OF TABLES

LIST OF FIGURES

LIST OF ABBREVIATIONS

GA	Genetic algorithm
CMS	Component mode synthesis

CHAPTER ONE

INTRODUCTION

In this chapter, engineering inverse problems identifying unknown structural properties such as the thickness of thin members and mass of a particle will be discussed. To solve the engineering inverse problem, a minimization constrained eigenvalue problem will be proposed. In addition, the method to solve the minimization constrained eigenvalue problems will also be described in detail in this chapter.

1.1 Engineering Inverse Problem

The inverse problem is one of the most critical problems studied in science and mathematics, as it can obtain some parameters that cannot be directly observed. It is found in system recognition, signal processing, medical imaging, computer vision, machine learning, non-destructive testing, and many other fields. A "direct problem" figures out how the phenomenon occurs, which can be calculated using tools like equations. However, the "inverse problem" will be processed based on the data contained in the phenomenon to estimate the nature of the object as some data are inevitably not present.

Consider a linear differential operator L of n^{th} order:

$$L(D; a_i)= a_n D^n+\cdots + a_1 D + a_0 \tag{1}$$

where a_j are system parameters and D^i is defined as

$$D^i=\frac{\partial^i}{\partial x_j^i} \tag{2}$$

Here, the variable x_j is a spatial coordinate or time. Further, a physical phenomenon may be governed by the following differential equation:

$$L(D; a_i)u_j = F_j \tag{3}$$

where u_j is the physical quantity to be determined when the input is given as F_j. For example, the vibration of a beam is governed by the following equation:

$$\left(EI\frac{\partial^4}{\partial x^2} + \rho A\frac{\partial^2}{\partial t^2}\right)v = F(x,t) \tag{4}$$

where E is the modulus of elasticity of the beam, I the moment of inertia of the cross-section, ρ the density, A the cross-sectional area, v the deflection, and $F(x,t)$ the lateral load applied on the beam.

In a regular problem, the system parameters a_i and the input function F are known with a set of adequately prescribed boundary conditions. The unknown variables u_j can be solved precisely or numerically. In a different class of problems, not all the system parameters are known, although the variables u_j are either known wholly or partially known through most practical means. Depending on the form the variables u_j provides, this type of problem is often known as an inverse problem or an ill-posed problem.

1.2 Vibrations Tuning

Tuning vibrations are frequently used in power transmissions, automobiles, and buildings. However, with the increase of internal and external excitations during the vehicle's operation, when the excitation frequency reaches the natural frequency of the vehicle, the vibration amplitude exceeds a specific range. As a result, vehicles are easily damaged due to resonance, and it may cause vehicle components to rupture and other early failure phenomena. These phenomena will affect the reliability and performance of the vehicle. In addition, long-term frequency vibration will significantly reduce comfort and cause the vehicle to emit harsh noises. To improve vehicle performance and meet the growing needs of automakers, research institutions are committed to solving this problem by adjusting the vibration to a particular range.

One way to tune the vibration is to adjust the vibration absorber. The tuned shock absorber proposed by Ormondroyd and den Hartog [1] has been used for many years. The equipment consists of a system with springs, masses, and shock absorbers, and the system's natural frequency can be adjusted by adding it to the host structure to reduce vibration. However, von Flotow [2] found that the tuned shock absorber sometimes deviated from the tuning position, resulting in a worse performance of the main structure. Brennan [3] also found that the atomized shock absorber may increase the vibration amplitude of its primary form. He developed a device that can adaptively adjust the shock absorber, avoiding misoperation by re-adjusting the shock absorber in real-time.

Another way to tune the vibration is to add a mass at a specific location on the structure, forming a constrained eigenvalue problem. Gander [4] introduced a method to solve the constrained Eigenvalue problem by eliminating linear constraints and minimizing them using the Lagrangian equation. Then, the problem can be reduced to an equation, which a conventional zero-finding process can solve. Salinas presented a model of the constrained eigenvalue problem for low energy modes [5]. His model is solved by using the ARPACK/PARPACK software in a shift-invert mode [6~7]. Christopher [1] provides an improved algorithm for solving numerical solutions of constrained symmetric eigenvalue problems based on the previous research. In another method, Y. M. Ram [3] proposed a way to solve constrained non-uniform linear eigenvalues and applied it to the problem of finding the frequency and amplitude of the exciting force that imposes constraints on the configuration of vibration modes.

In this dissertation, one or more masses will be added at specific locations on the structure to target natural frequencies. Then, a mathematical statement will be formulated for the problem in a constrained eigenvalue form and solve it using the Newton Raphson iteration and the genetic algorithm (G.A.).

1.3 Constrained eigenvalue problems

1.3.1 Eigenvalue problems

Let **A** and **B** be two transformation matrices, and **x** be an arbitrary vector. The vector **x** after the two transformations becomes, respectively,

$$\mathbf{y} = \mathbf{A}\mathbf{x} \tag{5}$$

and

$$\mathbf{z} = \mathbf{B}\mathbf{x} \tag{6}$$

When the two transformed vectors are parallel but different in length, they can be formatted as an eigenvalue problem. In mathematical terms, the eigenvalue problem can be described as,

$$\mathbf{A}\mathbf{x} = \lambda\mathbf{B}\mathbf{x} \tag{7}$$

where λ is a scalar, called the eigenvalue. For particular conditions, when B is an identity matrix, Eqn. (1) becomes the standard form of the eigenvalue problem:

$$\mathbf{A}\mathbf{x} = \lambda\mathbf{x} \tag{8}$$

The problem of eigenvalues appears in many engineering disciplines. For example, in mechanical engineering, eigenvalue problems are encountered when dealing with structural vibration. For an undamped system, the vibration is controlled by the following equation of motion:

$$\mathbf{M}\ddot{\mathbf{u}} + \mathbf{K}\mathbf{u} = \mathbf{F} \qquad (9)$$

where **M** and **K** are, respectively, the mass and stiffness matrices of the structure [4], **u** the nodal displacement vector, **ü** the nodal acceleration vector and **F** the nodal force vector. To determine the natural frequency, it is assumed that the system produces harmonic oscillations under free vibration, or **F** = 0. Thus,

$$\mathbf{u} = \mathbf{U}e^{i\omega t} \qquad (10)$$

where **U** is the amplitude of nodal displacement, $i = \sqrt{-1}$, ω the frequency of the harmonic function and t the time. Therefore, Eqn. (9) becomes:

$$(-\omega^2\mathbf{M} + \mathbf{K})\mathbf{U}e^{i\omega t} = \mathbf{0} \qquad (11)$$

For a non-trivial solution for **U** to exist, the determinant of the coefficient matrix must be zero. Thus,

$$\|\mathbf{K} - \lambda\mathbf{M}\| = 0 \qquad (12)$$

where $\lambda = \omega^2$, and $\|.\| = \det(.)$ is the determinant of a matrix. It is called the characteristic equation and can be used to determine the vibration system's natural frequencies and subsequent modes. Carrying out the determinant, Eqn. (12) becomes a polynomial in λ. Let function $f(\lambda)$ be:

$$f(\lambda) = \|\mathbf{K} - \lambda\mathbf{M}\| \qquad (13)$$

where λ is the root of the polynomial $f(\lambda)$. When the other parameters of the structure (such as point mass, thickness, Young's modulus, density, etc.) are considered, the above function can be written as,

$$f(\lambda, \eta) = \|\mathbf{K}(\eta) - \lambda\mathbf{M}(\eta)\| \tag{14}$$

where η is a relevant parameter of the structure.

Solving eigenvalue problems with effective numerical methods has become an important task. In structural vibration, the stiffness and mass matrices are always symmetrical. However, they may not be symmetrical in coupled-field problems, as seen in thermal-electrical [4] or thermal structural [5] areas. To solve the eigenvalue problem, several numerical methods have been developed. Von Mises [6] developed a numerical method called power iteration. The normalized value of matrix **A** is multiplied by the eigenvector of the previous iteration. A guessed eigenvector and an explicit guess of the eigenvalue are first obtained to calculate the eigenvector in the next iteration. The algorithm continues until a converged solution is achieved. Although power iteration is straightforward, the convergence tends to be slow. Pohlhausen [7] developed an inverse power method, producing convergent eigenvalues with a small number of iterations. Rayleigh [8] developed an iteration method using the Rayleigh quotient to obtain more accurate eigenvalues. After that, Francis [9] developed a Q.R. algorithm for decomposing a matrix into the product of an orthogonal matrix and an upper triangular matrix. Jacobi [10] developed an algorithm to calculate the eigenvalue for only real symmetric matrices. Cuppen [18] proposed a divide-and-conquer eigenvalue algorithm to ensure the stability and efficiency of the algorithm. However, the divide-and-conquer eigenvalue algorithm shows stability and efficiency in only a specific scope. If the condition lies outside the range, the algorithm becomes unstable. Then, the APRACK algorithm [6], used to solve large-scale Hermititian, non-Hermititian, standard, or generalized eigenvalue problems was developed. However, the APRACK solution does not work in solving nonsymmetric matrices or systems that are poorly conditioned. In these cases, a right-hand side method introduced by Bertille Claude [12] is used.

1.3.2 Constrained minimization problems

There are two kinds of constrained minimization problems, one with inequality constraint and the other with an equality constraint. A minimization problem with equality constraint can be expressed as below:

$$\min_{x} f(x)\,, \qquad \text{subject to} \qquad g(x) = 0. \tag{15}$$

For example, when $f(\,x_1,\,x_2) = x_1^2 + x_2^2,\ \ g(\,x_1,\,x_2) = x_2 + x_1 + 1$, Eqn. (15) becomes a minimization problem that calculates the minimum value through the intersecting curve of the surface of the elliptic paraboloid, as shown in Figure 1. The minimization problem can be written in the following form:

$$\min_{x_1}[x_1^2 + x_2^2]\ \ , \qquad \text{subject to} \qquad x_2 + x_1 + 1 = 0 \tag{16}$$

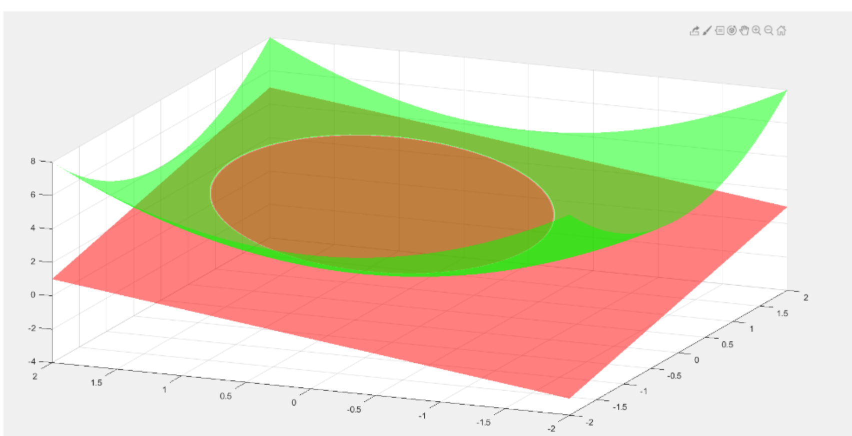

Figure 1. Minimization problem with equality constraint

An inequality constrained minimization problem can be stated as:

$$\min_{x} f(x) \quad , \qquad \text{subject to} \qquad x_{min} < x < x_{max} \tag{17}$$

For example, when $f(x) = 3x^2 - 5,\ x_{min} = 1,\ x_{max} = 2,$ Eqn. (17) becomes a problem that calculates the minimum of the parabola in the region of $1 < x < 4$, as shown in Figure 2. The example yields the following form:

$$\min_{x}(3x^2 - 5) \ , \qquad \text{subject to} \qquad 1 < x < 4 \tag{18}$$

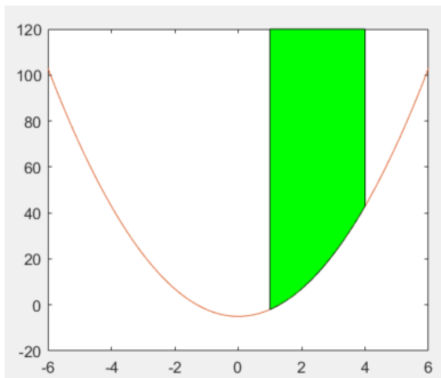

Figure 2. Minimization problem with an inequality constraint

One of the popular methods in linear programming is the Simplex method [13]. Moreover, ways to solve nonlinear optimization problems under constrained conditions include Lagrangian multipliers, penalty methods, and Newton methods [14~16].

1.3.3 Constrained eigenvalue problem

Some applications involving constrained eigenvalue problems include material property identification, vibration adjustment, etc., [22]. The methodology of solving constrained eigenvalue problems can be used to find unknown parameters of the structure, such as density, Young's modulus, sheet thickness, point mass, by predefining tolerance of the error between the calculated natural frequencies and the measured natural frequencies of the structure by hammer impacting test. To determine the unknown parameters of the structure η_i, the following constrained eigenvalue problem must be solved.

$$\|\mathbf{K}(\eta_i) - \omega^2\mathbf{M}(\eta_i)\| = 0, i = 1,2, \dots, p \tag{19}$$

subject to

$$\omega_j = \overline{\omega}_j,\ j = 1,2, \dots, q \tag{20}$$

where $\overline{\omega}_j$ are the measured natural frequencies, p the number of unknown parameters, and q the number of measurements. To solve the constrained eigenvalue problem[24], the following equation will be derived. Recall from Eqn. (14),

$$f(\lambda, \eta) = \|\mathbf{K}(\eta) - \lambda\mathbf{M}(\eta)\| \tag{21}$$

Thus, the following constrained minimization problem can be formed,

$$\min_{\lambda,\eta} f(\lambda, \eta) \qquad \text{subject to} \quad \lambda = \bar{\lambda}_1 \tag{22}$$

In this study, constraints were imposed on the eigenvalues, which contrasts with the constraints on eigenvectors found in the previous work. For example, in the work by Baker and Lehoucq [24], the constrained eigenvalue problem is described as:

$$\left(\begin{bmatrix} \mathbf{A} & \mathbf{B}^\mathbf{T} \\ \mathbf{B} & \mathbf{0} \end{bmatrix} - \lambda \begin{bmatrix} \mathbf{C} & \mathbf{0} \\ \mathbf{0} & \mathbf{0} \end{bmatrix}\right) \begin{Bmatrix} \mathbf{u} \\ \mathbf{v} \end{Bmatrix} = \mathbf{0} \tag{23}$$

where **A** is the stiffness matrix, **B** the constraint matrix, and **C** the mass matrix, the second equation represents a constraint imposed on the part of the displacement vector. That is, the constraint is

$$\mathbf{Bu} = \mathbf{0} \tag{24}$$

In vibration, matrix **A** and matrix **C** are, respectively, the stiffness and mass matrices. For example, in the hinged roller beam shown in Figure 3, the roller at C is constrained to move in the oblique direction. The constraint for the node is given as follows,

$$u_c \tan\beta - v_c = 0 \qquad (25)$$

where β is the angle of the incline, and u_c and v_c are, respectively, the *x*- and *y*-displacements of point C. Thus, the above constrained equation can be written in matrix form.

$$\lfloor \tan\beta \quad -1 \rfloor \begin{Bmatrix} u_c \\ v_c \end{Bmatrix} = 0 \qquad (26)$$

which can be readily incorporated into the final system of the model.

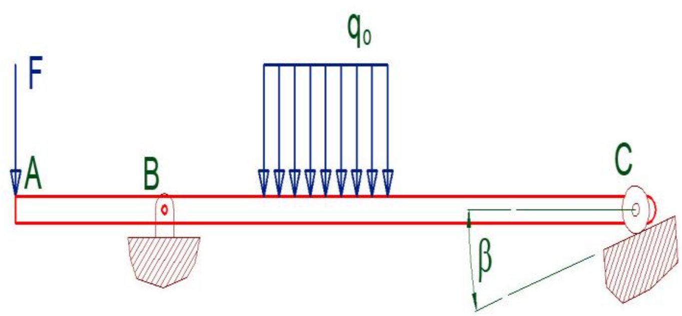

Figure 3. A hinged-roller beam on an incline at C.

CHAPTER TWO

SOLUTION METHODS FOR CONSTRAINED EIGENVALUE PROBLEMS

2.1 Introduction

There are various methods for solving a constrained eigenvalue problem [15, 21]. In this research, the Newton-Raphson iteration method and genetic algorithm (G.A.) were selected. The Newton-Raphson iteration method is a direct method, which can be used to calculate the slope of the equation curve and generate a new conjecture solution until some convergence criteria are used to prove that the new conjecture solution is the best, thereby finding a solution. Although the Newton-Raphson iteration can find an answer in a short period, there are still some shortcomings. Since the Newton-Raphson iteration is a direct method, it is highly dependent on the target equation, which may slow down or stagnate the solution process at specific points in the region. A genetic algorithm is proposed to overcome this shortcoming when the Newton-Raphson iterative process is slow or does not produce a convergent solution. Genetic algorithm is an indirect method, so it does not depend on the target equation. However, compared with the Newton-Raphson iteration method, the genetic algorithm usually takes longer to obtain a satisfactory solution. This is because it generates new or multiple guesses that are not related to the target equation. In this research, both the Newton-Raphson iteration method and the Genetic algorithm are employed to solve the problems.

2.2 Mathematical formulation of constrained eigenvalue problem

Let's first consider a simple case of the constrained eigenvalue problem in which there is only one unknown parameter to be determined and only one measured natural frequency has been obtained. That is, p = q = 1. The constrained eigenvalue problem posed in Eqns. (19) and (20) may be restated in the following form.

$$\|\mathbf{K}(\eta) - \omega^2\mathbf{M}(\eta)\| = 0 \tag{27}$$

$$\omega - \bar{\omega}_1 = 0. \tag{28}$$

Clearly, they represent a system of two equations one of which is highly nonlinear. For developing a solution algorithm for this simple case, let f_1 and f_2 be defined as:

$$f_1 = \omega - \bar{\omega}_1, \tag{29}$$

$$f_2 = \|\boldsymbol{K}(\eta) - \omega^2\boldsymbol{M}(\eta)\| \tag{30}$$

Symbolically, they can be represented in the following form.

$$f_i(x_j) = 0, \tag{31}$$

where x_j are the unknown eigenvalue ω and the system parameter η. The approach to solve the above system of nonlinear equations is presented in the next section.

In the case of a more complicated case where $p > 1$ and $q > 1$, an error function is first constructed in the following way.

$$e_d = \sum_{j=1}^{q} \frac{1}{2}\left(\left\|\mathbf{K}(\eta_i) - \bar{\lambda}_j\mathbf{M}(\eta_i)\right\|\right)^2, \tag{32}$$

where, the known eigenvalues $\bar{\lambda}_j$ are determined from the measured natural frequencies $\bar{\omega}_j$ via the following relation.

$$\bar{\lambda}_j = \bar{\omega}_j^2. \tag{33}$$

In addition, each term in the summation represents the error of the determinant stemming from using one $\bar{\lambda}_j$ and a set of estimated values for unknown parameters η_i. Naturally, we must have the condition that the number of unknown parameters must not exceed the number of measurements. That is, the relation $p \leq q$ must hold. Further, as in many minimization schemes [21], the fraction ½ is inserted in the above for easy manipulation in the future.

A second error function may be constructed by considering Rayleigh quotient which is a well-known term in linear algebra, matrix computations and numerical methods [15~17]. Let $\mathbf{\Phi}$ be the modal matrix of the eigensystem consisting of the usual mass and stiffness matrices $\mathbf{M}$ and $\mathbf{K}$, respectively. Thus, we have,

$$\bar{\mathbf{K}} = \mathbf{\Phi}^{\mathrm{T}}\mathbf{K}\mathbf{\Phi}, \qquad \bar{\mathbf{M}} = \mathbf{\Phi}^{\mathrm{T}}\mathbf{M}\mathbf{\Phi} \tag{34}$$

where both $\bar{\mathbf{K}}$ and $\bar{\mathbf{M}}$ are diagonal matrices. In case the modal matrix is orthonormalized with respect to the mass matrix, $\bar{\mathbf{M}}$ is an identity matrix $\mathbf{I}$, while the diagonal components of $\bar{\mathbf{K}}$ are the eigenvalues. In any event, we have the following Rayleigh quotient.

$$\lambda_j = \frac{\boldsymbol{\phi}_j^T\mathbf{K}\boldsymbol{\phi}_j}{\boldsymbol{\phi}_j^T\mathbf{M}\boldsymbol{\phi}_j} \tag{35}$$

where $\boldsymbol{\phi}_j$ is the j-th eigenvector in $\mathbf{\Phi}$. With the Rayleigh quotient now given, the alternative error function is defined in the following manner.

$$e_r = \sum_{j=1}^{q}\frac{1}{2}\left(\lambda_j - \bar{\lambda}_j\right)^2 = \sum_{j=1}^{q}\frac{1}{2}\left(\frac{\boldsymbol{\phi}_j^T\mathbf{K}\boldsymbol{\phi}_j}{\boldsymbol{\phi}_j^T\mathbf{M}\boldsymbol{\phi}_j} - \bar{\lambda}_j\right)^2, \tag{36}$$

Here, λ_j is calculated using a set of estimated values for the unknown parameters and $\bar{\lambda}_j$ is the same as in Eqn. (33). In the next session, a minimization scheme is shown to find the unknowns parameters η_i.

2.3 Minimization of error function

In the previous section, a pair of error functions are defined. In essence they represent the difference between the empirical value and its counterpart obtained numerically by using guessed values for the unknown parameters in the mathematical model. Therefore, our goal is to find the unknown parameters, so the error is smaller than a predefined tolerance, if not equal to zero. The mathematical description can be stated as follows.

$$\min_{\eta_i} e_d \tag{37}$$

where the error function given in Eqn. (32) is considered first.

Employing the technique widely available for minimization, we set the gradient of the error function equal to zero.

$$\nabla e_d = 0, \tag{38}$$

which is known as the stationary condition for a minimum [21]. Introducing the error function into Eqn. (38), the following system of nonlinear equations is reached.

$$\sum_{j=1}^{q} f_j \frac{\partial f_j}{\partial \eta_i} = 0, i = 1,2, \dots, p, \tag{39}$$

where f_j is the determinant of the eigensystem as given below.

$$f_j = \left\| \mathbf{K}(\eta_i) - \bar{\lambda}_j \mathbf{M}(\eta_i) \right\|, \tag{40}$$

For brevity in the development, the following notation is adopted.

$$\mathbf{A}_j(\eta_i) = \mathbf{K}(\eta_i) - \bar{\lambda}_j \mathbf{M}(\eta_i), \tag{41}$$

As indicated in Eqn. (39), the derivative of a determinant is warranted. According to Jacobi's formula [24] the derivative of the determinant is given as,

$$\frac{\partial}{\partial \eta_i} \det\left(\mathbf{A}_j(\eta_i)\right) = \det\left(\mathbf{A}_j(\eta_i)\right) tr\left(\mathbf{A}_j^{-1}(\eta_i) \frac{\partial}{\partial \eta_i} \mathbf{A}_j(\eta_i)\right), \tag{42}$$

where tr() signifies the trace of the matrix. The system of nonlinear equations Eqn. (39) can be written as below.

$$\sum_{j=1}^{q} \left[\det\left(\mathbf{A}_j(\eta_i)\right)\right]^2 tr\left(\mathbf{A}_j^{-1}(\eta_i) \frac{\partial}{\partial \eta_i} \mathbf{A}_j(\eta_i)\right) = 0, \qquad i = 1,2,\dots,p. \tag{43}$$

It is readily seen that the above system of nonlinear equations is rather complicated and poses numerical challenges even in a mid-sized model. The primary issue lies in the evaluation of the determinant of a large matrix. The details are to be presented in the later sections where several actual models with various settings are dealt with.

2.4 Minimization using genetic algorithm

Genetic algorithm (G.A.) [17]-[19] initially generates a set of applicant solutions that represent the answer to the optimization problem from the beginning. Each solution is a potential applicant for the optimization of the optimization problem. Then, by using fitness-based methods (more likely to choose more suitable solutions), it selects a portion of the population to propagate the new generation. Certain selection methods will evaluate the applicability of each solution and prioritize the best solution. They are usually a list of values and are usually more based on a set of symbols. Then, the next step is to generate next-generation solutions through crossover and mutation.

For each fresh solution to be created, the pair of solutions selected for breeding from the previously selected population is the "parent". Then, the "parent" solution uses mutation and crossover to generate the " children " solution. The "children" solution has many "parent" characteristics. This process continues until a new group of best solutions is created. The two error functions e_d and e_r presented in the previous sections, Eqns. (32) and (36), are to be minimized using G.A. to determine the unknown parameters η_i. In particular the error function e_r in Eqn. (36) was formed for G.A. minimization. Thus, there is no further mathematical treatment on e_r after it is defined.

2.5 Newton-Raphson iteration

Newton-Raphson iteration method remains a widely numerical technique for solving for the roots of a system of nonlinear equations [15]. The method is relatively simple and accurate which has been widely used in many applications. As opposed to secant, false position methods, and the others, Newton-Raphson iteration requires only one starting point, the initial guess. A brief description of the method is given below. In this study, there are two systems of nonlinear equations formulated, Eqns. (31) and (43). They can be represented in the following general form.

$$F_j(x_i) = 0, \tag{44}$$

where x_i are the unknown variables. In the iterative scheme, an improvement at the *k*-th step is calculated via the following equation.

$$\Delta x_i^{(k)} = -\left[\left(\frac{\partial F_j}{\partial x_i}\right)^{(k)}\right]^{-1} F_j\left(x_i^{(k)}\right). \tag{45}$$

The updated unknown $x_i^{(k+1)}$ is obtained by the following relation.

$$x_i^{(k+1)} = x_i^{(k)} + \Delta x_i^{(k)}. \tag{46}$$

A preset tolerance ε is selected to terminate the iteration when the following condition is met.

$$\left|\frac{\Delta x_i^{(k)}}{x_i^{(k+1)}}\right| < \varepsilon. \tag{47}$$

It is worth noting that in Eqn. (45) the partial derivative term inside the bracket, $\frac{\partial F_j}{\partial x_i}$, is known as Jacobian matrix or the gradient of the function. It is apparent that calculating the Jacobian matrix for the system of nonlinear of equations in Eqn. (43) requires much greater efforts than that for the system in Eqn. (31). Further, calculating Jacobian matrix is not required in the other numerical methods for roots finding.

A MATLAB code cEVP.m is developed based on the proposed algorithm for solving constrained eigenvalue problems. MATLAB program is selected due to its availability of a wide range of callable routines. In the following sections, a discrete spring-mass system, a cantilever beam, a plane frame, and a frame fabricated using a thin plate are chosen to show the effectiveness and accuracy of the algorithm. The numerical difficulties encountered and the overcoming remedies are also presented. To further validate the proposed novel technique, empirical work is set up to demonstrate a couple of examples involving a cantilever beam and a frame fabricated using a thin plate.

CHAPTER THREE

NUMERICAL APPLICATIONS

3.1 Introduction

To verify the effectiveness of the algorithm, we will consider some numerical examples, including discrete systems and continuous systems. In the part of the discrete system, we will propose a spring-mass system as a numerical application. However, in the continue systems part, we will apply the most practical engineering structures: beam structure, frame structure, and plate structure with unknown parameters such as Young's modulus, density, and particle in a particular place. Details of identifying the unknown parameters of the structure using the natural frequencies will be described in this chapter. The finite element method was used to build the mathematical models of the spring-mass system, beam structure, frame structure, and plate structure before determining the unknown parameters.

3.2 Spring-mass system

In a dynamical system study, it is customary to simplify the dynamical system into two models, discrete system and continuous system, to reduce the complexity and make the study more effective. Although all the dynamical systems are composed of continuous elements, some dynamical systems like the mass-spring obeys the character of the discrete system, so we simplify that dynamical system as discrete system [26].

Consider a discrete spring-mass system as shown in Figure 4 with stiffness parameters from k_1 to k_{n+1} and mass parameters from m_1 to m_n. Moreover, the first natural frequency of the spring-mass system is ω_1. To determine one unknown stiffness parameter k_j or mass parameter m_j, inverse algorithm can be applied based on the known first natural frequency of the spring-mass system ω_1 and other known stiffness parameters or mass parameters. Before this, the mathematical model of this spring-mass system will be established based on the finite element method through the stiffness matrix $\mathbf{K}(k_j)$ and mass matrix $\mathbf{M}(m_j)$ given in Eqn (104) in Appendix.

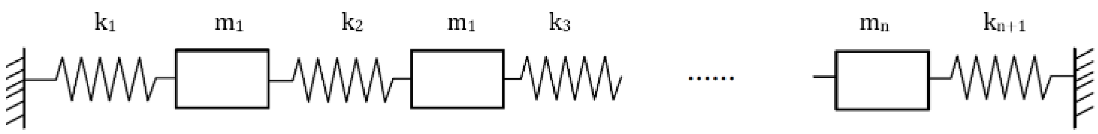

Figure 4. An n-DOF discrete system

3.2.1 Determine unknown stiffness parameter k_j

The mathematical model of the spring-mass system was demonstrated as below:

$$F(k_j) = \left\| \mathbf{K}(k_j) - \omega_1^2 \mathbf{M} \right\| \tag{48}$$

where $\mathbf{K}(k_j)$ is the stiffness matrix, and $\mathbf{M}$ is the mass matrix.

Newton's iteration was applied to determining the unknown parameter by improving the guessed value in each iteration until it met the preset condition. Recall Eqn. (45), in calculating the improvement at each step, $\frac{\partial \mathrm{F}(k_j)}{\partial k_j}$ is a constant value that can be obtained after achieving the value of $\frac{\partial \mathbf{M}}{\partial k_j}$ and $\frac{\partial \mathbf{K}(k_j)}{\partial k_j}$. Note that $\frac{\partial \mathbf{M}}{\partial \rho}$ is a zero matrix for the **M** matrix remain the same in each iteration, $\frac{\partial \mathbf{K}(k_j)}{\partial k_j}$ is a nonzero matrix for the **K** matrix was changing in every iteration and can be calculated numerically. In order to calculate $\frac{\partial \mathbf{K}(k_j)}{\partial k_j}$, we firstly set two different numerical values, such as 0 and 1, to k_j in

$\mathbf{K}(k_j)$ matrix in turn as $\mathbf{K_1}$ matrix, and find all the nonzeros elements k_{ab} of the $\mathbf{K_1}$ matrix.

$$\mathbf{K_1} = \mathbf{K}(1) - \mathbf{K}(0) \tag{49}$$

Then, $\frac{\partial \mathbf{K}(k_j)}{\partial k_j}$ is equal to the $\mathbf{K_1}$ matrix that all the nonzeros elements k_{ab} are set to 1. After that, Newton's iteration will start to work and then be terminated when the preset condition is met. If the preset conditions are not met after specific iterations, GA will be used to determine k_j of the spring-mass system as an alternative algorithm. Prior to solving it using GA, an error function $e_d(k_j)$ was set as below:

$$e_d(k_j) = \left\|\boldsymbol{K}(k_j) - \varpi_1^2 \boldsymbol{M}\right\| \tag{50}$$

where $\mathbf{K}(k_j)$ is the stiffness matrix, and $\mathbf{M}$ is the mass matrix, k_j is the unknown stiffness parameter of the spring-mass system. After the function $e_d(k_j)$ is formed, an upper bound and lower bound for the unknown parameter k_j could be provided as a guessed limitation to reduce computational complexity. Finally, the unknown parameter k_j will be identified using a MATLAB code basing on the GA algorithm.

<u>3.2.2 Determine unknown mass parameter m_j</u>

The mathematical model of the spring-mass system can be demonstrated as below:

$$F(m_j) = \left\|\mathbf{K} - \varpi_1^2 \mathbf{M}(m_j)\right\| \tag{51}$$

where $\boldsymbol{K}$ is the stiffness matrix, and $\mathbf{M}(m_j)$ is the mass matrix, m_j is the unknown mass parameter of the spring-mass system.

Newton's iteration was applied to determining the unknown parameter by improving the guessed value in each iteration until it met the preset condition. Recall Eqn. (45), in calculating the improvement at each step, $\frac{\partial F(m_j)}{\partial m_j}$ is a constant value that can be obtained after achieving the value of $\frac{\partial \mathbf{K}}{\partial m_j}$ and $\frac{\partial \mathbf{M}(m_j)}{\partial m_j}$. $\frac{\partial \mathbf{K}}{\partial m_j}$ is a zero matrix for the **K** matrix remain the same in each iteration, $\frac{\partial \mathbf{M}(m_j)}{\partial m_j}$ is a nonzero matrix for the **M** matrix was changing in every iteration and can be calculated numerically. In order to calculate $\frac{\partial \mathbf{M}(m_j)}{\partial m_j}$, we firstly set two different numerical values, such as 0 and 1, to m_j in $\mathbf{M}(m_j)$ matrix in turn as $\mathbf{M_1}$ matrix, and find all the nonzeros elements m_{ab} of the $\mathbf{M_1}$ matrix.

$$\mathbf{M_1} = \mathbf{M}(1) - \mathbf{M}(0) \quad (52)$$

Then, $\frac{\partial \mathbf{M}(m_j)}{\partial m_j}$ is equal to the $\mathbf{M_1}$ matrix that all the nonzeros elements m_{ab} are set to 1. After that, Newton's iteration will start to work and then be terminated when the preset condition is met. If the preset conditions are not met after specific iterations, GA will be used to determine m_j of the spring-mass system as an alternative algorithm. Prior to solving it using GA, an error function $e_d(m_j)$ was set as below:

$$e_d(m_j) = \left\|\mathbf{K} - \bar{\omega}_1^2 \mathbf{M}(m_j)\right\| \quad (53)$$

where **K** is the stiffness matrix, and $\mathbf{M}(m_j)$ is the mass matrix, m_j is the unknown mass parameter of the spring-mass system. After the function $e_d(m_j)$ is formed, an upper bound and lower bound for the unknown parameter m_j could be provided as a guessed limitation to reduce computational complexity. Finally, the unknown parameter m_j will be identified using a MATLAB code basing on the GA algorithm.

3.2.3 A numerical example for spring-mass system

Consider a discrete spring-mass system as shown in Figure 4, m_1 is an unknown parameter of this system, and the following parameters are known: n = 20, k_1 = 100 kN/m, k_2 = 400 kN/m, k_3= 200 kN/m, the stiffness of the remaining springs are all equal to 800 kN/m. Further, the second mass of the block m_2 = 6 kg, the remaining blocks are 2 kg each, and the first natural frequency ω_1 is 10.32 Hz. Therefore, our goal is to determine the unknown mass of the first block m_1. Before using Newton's method to get the unknown, we must first give a guessed value. We set the guessed value to 10 kg. Through calculations, the unknown block m_1 was determined using Newton's method in only three iterations, and the results are shown in Table 1.

Table 1. The result of predicted mass, unit: kg for mass.

Mass Predicted	Actual Mass	Error
8.0003	8	0

3.3 Beam structure

Beam is one of the essential components that make up various structures, and it is the most widely used bending structure in engineering, such as beam bridges and building beam-column systems. The use of beam structure can be traced back to the bamboo-wood beam bridge of prehistoric humans. There are two popular beam theories: Euler–Bernoulli beam theory and Timoshenko beam theory. The Euler–Bernoulli beam theory, developed around 1750, is mainly applied in the beam structures under axial forces and bending. It came with two primary assumptions. First, the plane sections remain plane, which suggests that any section of a beam perpendicular to the neutral axis before the beam deforms will remain perpendicular to the neutral axis after the beam deforms. Second, deformed beam angles are small after the beam deforms. However, Timoshenko's beam theory assumptions are based on the Euler–Bernoulli beam theory hypothesis, but it also counts transverse shear strain which is the difference between the rotation of transverse normal and the slope of the beam. The following section will discuss the applications of the inverse algorithm of two beam structures: a cantilever beam and a fixed-hinged beam.

3.3.1 Cantilever beam

A cantilever beam is a structural beam supported at one end and freed at the other end. Consider a cantilever beam of length L, cross-section $b \times h$, the density ρ and Young's modulus E. The distance between point A and the location of the particle is as shown in Figure 5. The first natural frequency of the beam is ω_1. If one of the parameters of the cantilever beam is unknown, an inverse algorithm was used to determine it. The cantilever beam's mathematical model was built with the finite element method using the mass matrix and stiffness matrix in Eqn. (105) and (106) in Appendix, and the first natural frequency of the beam ω_1 can be obtained according to Eqn.(12) after all the matrices were assembled. The density ρ, Young's modulus E, and the particle's mass installed on the beam m will be determined using Newton's iteration and GA in the following section.

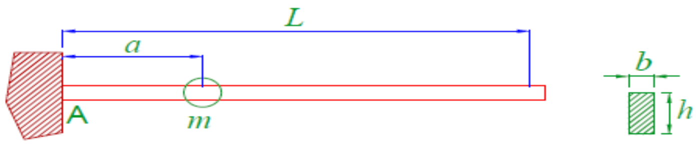

Figure 5. A cantilever beam with a particle

3.3.1.1 Determine density of cantilever beam

Since the length L, cross-section $b \times h$, Young's modulus E, and installed particle m of the cantilever beam are known parameters and density ρ is an unknown parameter. The mathematical model of the cantilever beam can be demonstrated as below:

$$F(\rho) = \|\mathbf{K} - \bar{\omega}_1^2 \mathbf{M}(\rho)\| \tag{54}$$

where $\mathbf{K}$ is the stiffness matrix, and $\mathbf{M}(\rho)$ is the mass matrix.

Finding an unknown number in the beam structure is similar to the method used in the discrete system. Newton's iteration was applied to determine the unknown parameter by improving the guessed value in each iteration until it met the preset condition. Recall Eqn. (45), in calculating the improvement at each step, $\frac{\partial F(\rho)}{\partial \rho}$ is a constant value that can be obtained after achieving the value of $\frac{\partial \mathbf{K}}{\partial \rho}$ and $\frac{\partial \mathbf{M}(\rho)}{\partial \rho}$. $\frac{\partial \mathbf{K}}{\partial \rho}$ is a zero matrix for the $\mathbf{K}$ matrix remain the same in each iteration, $\frac{\partial \mathbf{M}(\rho)}{\partial \rho}$ is a nonzero matrix for the $\mathbf{M}$ matrix was changing in every iteration and can be calculated numerically according to the Eqn.(52). After that, Newton's iteration will start to work and then be terminated when the preset condition is met. If preset conditions are not met after specific iterations, GA will be used to determine the density ρ of the cantilever beam as an alternative algorithm that is the same as mentioned in the spring-mass system section with the error function $e_d(\rho)$ as shown in Eqn.(53).

3.3.1.2 Determine mass m of a particle installed on a cantilever beam

Determining mass m of a particle installed on a cantilever beam is similar as mentioned in the last section to determining the density of the beam that calculates the improvement at each step using Newton's iteration. To obtain the improvement at each step, $\frac{\partial \mathbf{F}(m)}{\partial m}$ needs to be found by achieving the value of $\frac{\partial \mathbf{K}}{\partial \mathrm{m}}$ and $\frac{\partial \mathbf{M}(\mathrm{m})}{\partial \mathrm{m}}$, $\frac{\partial \mathbf{K}}{\partial \mathrm{m}}$ is a zero matrix, $\frac{\partial \mathbf{M}(\mathrm{m})}{\partial m}$ is a nonzero matrix for the **M** matrix was changing in every iteration and can be calculated numerically. The process of calculating $\frac{\partial \mathbf{M}(\mathrm{m})}{\partial \mathrm{m}}$ is similar as mentioned in the last section according to Eqn.(49). After the value of $\frac{\partial \mathbf{F}(m)}{\partial m}$ is obtained, Newton's iteration will work and then be terminated when the preset condition is met. If the preset conditions are not met after specific iterations, GA will be used as an alternative algorithm with an error function $e_d(m)$ according to Eqn.(53).

3.3.1.3 Determine the location of a particle installed on a cantilever beam

Determine the specific location of a particle installed on a cantilever beam is a bit different from finding the density of the beam mentioned in the previous section. In each iteration, the stiffness matrix and mass matrix of the mathematical model of the beam are different. Moreover, the improved position of the particle in each iteration is possible not to be included in the nodes that have been meshed. So, in each iteration, the beam structure needs to be re-meshed according to the improved position of the particle. To save the calculation time, a technique that re-meshes a few points close to the improved position of the particle and keeps the other points unchanged is also used. Moreover, a numerical technique called moving finite element analysis was also applied and elaborated in the next section to make the mesh smoothly.

3.3.1.3.1 Moving finite element analysis Miller originally introduced the moving finite element method in 1981 as an adaptive mesh method solution in which the finite element mesh is continuously deformed over time [32], [33]. Then, it has been widely used in a large number of problems in science and engineering. These problems involve time-dependent partial differential equations that describe solutions that have significant spatial activity in a region of space that moves with time. After that, Gu[34] developed the moving finite element analysis to tackle the indentation of elastic beams whose closed-form solutions exist which is suitable to all similar questions about beam structures.

3.3.1.3.2 Determine the location of a particle using moving finite element analysis

Consider a beam BCD with the length w as shown Figure 6, point B and point D are ends of the beam, a particle was placed at point C that is a away from the point B. In order to simplify the process of the calculation, a natural coordinate is defined in the following way. Assuming that x is any length of the original coordinate, ξ is the corresponding natural coordinate. Obviously, $0 \leq x \leq w$ and $-1 \leq \xi \leq 1$. So x and ξ satisfy the following relationship:

$$\xi = \begin{cases} \dfrac{x-a}{a}, & 0 \leq x < a \\ \dfrac{x-a}{w-a}, & a \leq x < w \end{cases} \tag{55}$$

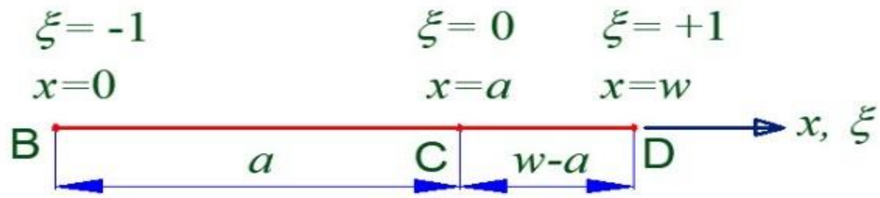

Figure 6. Natural coordinate.

Before the numerical execution, the natural coordinates of all nodes on the BCD are determined based on the initial guess of a. The natural coordinates of their nodes remain unchanged throughout the iteration. And the mass matrix and stiffness matrix are calculated again according to the new node x coordinate after the re-mesh. Once the convergent solution is reached, the node x coordinate can be calculated using the inverse form of the Eqn.(55). However, in some complex cases, especially in the case that contains a very large number of nodes, this method will consume a lot of calculation time. Because in each iteration of the excution inverse algorthm of beam structure, the stiffness matrix and the mass matrix are recalculated. In order to reduce the calculation time and the complexity of the inverse problem, in some complex problems, we apply this technique to the interest range that near the guessed loaction in each iteration. So in this case, the natural coordinate becomes:

$$\xi = \begin{cases} \dfrac{x-a}{a}, & a - a_1 \leq x < a \\ \dfrac{x-a}{w-a}, & a \leq x < a + a_1 \end{cases} \tag{56}$$

where a_1 is half the length of the range of interest, and $a - a_1 \leq x \leq a + a_1$ and $-1 \leq \xi \leq 1$. The numerical value of a_1 could be obtained as the sum length of the *n* elements of the original meshed beam that located before the initial guess location. If the guessed position to the position of point B is less than a_1, then the natural coordinate becomes:

$$\xi = \begin{cases} \dfrac{x-a}{a} - 2, & 0 \le x < a \\ \dfrac{x-a}{a_1 - a} - 2, & a \le x < a_1 \end{cases} \tag{57}$$

where $0 \le x \le a_1$ and -3 ≤ ξ ≤-1. If the guessed position to the position of point B is greater than $w - a_1$, then the natural coordinate becomes:

$$\xi = \begin{cases} \dfrac{x-a}{a} + 2, & w - a_1 \le x < a \\ \dfrac{x-a}{w - a_1} + 2, & a \le x < w \end{cases} \tag{58}$$

where $w - a_1 \le x \le w$ and 1 ≤ ξ ≤3.

So the natural coordinate for the complex problem is:

$$\xi = \begin{cases} \dfrac{x-a}{a} - 2, & 0 \le x < a, a < a_1 \\ \dfrac{x-a}{a_1 - a} - 2, & a \le x < a_1, a < a_1 \\ \dfrac{x-a}{a}, & a - a_1 \le x < a, a > a_1 \\ \dfrac{x-a}{w-a}, & a \le x < a + a_1, a > a_1 \\ \dfrac{x-a}{a} + 2, & w - a_1 \le x < a\ , a > w - a_1 \\ \dfrac{x-a}{w - a_1} + 2, & a \le x < w, a > w - a_1 \end{cases} \tag{59}$$

where $0 \le x \le w$ and -3≤ ξ ≤3.

After the natural coordinate system is determined, finding the location of a particle installed on a cantilever beam can be implemented. The process is similar as mentioned in the last section, to determine the beam's density that calculates the improvement at each step using Newton's iteration. Using Eqn.(56) as the natural coordinate system if the target system is relatively simple. If the target system is more complex, use Eqn.(59) as the natural coordinate system. Then, the length of each element ΔL can be obtained from the developed particle position in each iteration through the natural coordinate. To obtain the improvement at each step, $\frac{\partial \mathbf{F}(\Delta L)}{\partial \Delta L}$ needs to be found by achieving the value of $\frac{\partial \mathbf{K}(\Delta L)}{\partial \Delta L}$ and $\frac{\partial \mathbf{M}(\Delta L)}{\partial \Delta L}$. After the value of $\frac{\partial \mathbf{F}(\Delta L)}{\partial \Delta L}$ is obtained, Newton's iteration will work and then be terminated when the preset condition is met. If preset conditions are not met after specific iterations, GA will be used as an alternative algorithm with an error function $e_d(\Delta L)$ according to Eqn.(53).

3.3.1.4 A numerical example for a cantilever beam

Consider a cantilever beam as shown in Figure 5 with length L = 0.45 m, cross-section b×h= 31×1.34mm, the density of ρ = 7727kg/m3, Young's modulus of 210 GPa, and a particle placed on the beam with unknown mass m. The distance between point A and the location of the particle is 170 mm. The first natural frequency ω_1 is 5.477 Hz, and our goal is to determine the unknown mass of the particle placed on the beam m. Before using Newton's method to get the unknown, we must first give a guessed value of 1g. Through calculations, the unknown mass of the particle placed on the beam m was determined using Newton's method in only three iterations shown in Table 2. Then we set the particle's mass placed on the beam to 30g, and the density is an unknown parameter ρ. Through calculations, Newton's iteration determined the unknown mass of the particle placed on the beam m. However, Newton's iteration did not converge within 50000 iterations, so GA will be applied as an alternative algorithm, and the results are shown in Table 3.

Table 2. The result of predicted mass, unit: g for mass.

Mass Predicted	Actual Mass	Error
29.1	30	2%

Table 3. The result of predicted density, unit: g for mass.

Density Predicted	Actual Density	Error
7725.28	7727	0.02%

If the mass of the particle is known, the location of particle can also be determined by the reverse algorithm. Before using Newton's method to get the unknown, we must first give a guessed value of 100m. Through calculations, the unknown location of the particle placed on the beam *a* was determined using Newton's method in 18 iterations shown in Table 4.

Table 4. The result of predicted location of particle, unit: m for location for the particle (the fixed end of the beam is the origin of the coordinate), unit: m for location.

Location Predicted	Actual Location	Error
0.168	0.17	1%

3.3.2 Fixed-hinged beam

Consider a fixed-hinged beam of length L, cross-section $b \times h$, the density ρ and Young's modulus E. The beam is fixed at one end at point A and hinged at the other end at point B with a particle m installed. The distance between point A and the location of the particle is as shown in Figure 7. The first natural frequency of the beam is ω_1. If one of the parameters of the cantilever beam is unknown, an inverse algorithm can be used to determine it. The fixed-hinged beam's mathematical model can be built using the finite element method using the mass matrix and stiffness matrix in Eqns. (105) and (106) in Appendix, and the first natural frequency of the beam ω_1 can be obtained according to Eqn.(12) after all the matrices were assembled. Parameters like density, the mass of a particle installed on the beam m, and others can be determine using the proposed inverse algorithm. A numerical example will be provided in the following section.

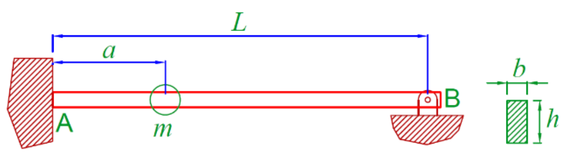

Figure 7. A fixed-hinged beam with a mass

3.3.2.1 A numerical example for a fixed-hinged beam

Consider a fixed-hinged beam as shown in Figure 7 with length L = 1m, cross-section $b \times h$= 20×20mm, density ρ = 7870 kg/m^3, Young's modulus of 200 GPa, and a particle placed on the beam with unknown mass m. The distance between point A and the location of the particle is 0.5m. The first natural frequency $\overline{\omega}_1$ is 24.682 HZ, and our goal is to determine the unknown mass of the particle placed on the beam *m*. Before using Newton's method to get the unknown, we set the guessed value to 1kg. Through calculations, the unknown mass of the particle placed on the beam *m* was determined using Newton's method in only three iterations shown in Table 5.

Table 5. The result of predicted mass, unit: kg for mass.

Mass Predicted	Actual Mass	Error
10	10	0

3.4 Frame structure

A frame structure combining beams and columns to resist lateral and gravity loads is usually used to overcome the significant moments due to the applied load. The two most common frame structures, plane frame and three-dimensional frame structures, will be introduced next. A plane frame is a two-dimensional structure composed of straight elements connected together by rigid and hinged connections. The frame bears loads and reaction forces in the structural plane. Three-dimensional frame, also known as a space beam, is a widely used in construction and structural engineering. It is a strong, lightweight truss-like structure that can transfer tensile and compressive loads from one point to another [37]. The proposed three-dimensional frame element is solved based on the Bernoulli-Euler beam theory [36], excluding shear deformation. Each element contains two nodes, and each node has six degrees of freedom. The stiffness matrix and mass matrix for each three-dimensional frame using the local reference system are shown as Eqn. (107) in Appendix A.

Cartesian reference transformation [40] technology will also be introduced to convert the local reference system into a global reference to assemble all the stiffness matrices and mass matrices. Then, the entire system's stiffness matrix and mass matrix can be obtained by combining each element's stiffness matrix and mass matrix. In this way, an unknown parameter or parameters in a three-dimensional frame structure can be determined using Newton's iteration method or genetic algorithm.

3.4.1 Cartesian Reference Transformation

When the mass and stiffness matrices were assembled, they should be transformed from a local reference system to the global system. It is challenging to use only two nodes to identify the cross-sectional direction of each element. In the local reference system, the *X'*-axis identifies the direction of the long side of the three-dimensional frame element, and the *Y'*-axis and *Z'*-axis are used to determine the cross-sectional direction of the three-dimensional frame element. Therefore, when transforming the element to the global system, a third node of the three-dimensional frame element need to be introduced to locate the Z'-axis in the local reference system. We set the coordinate of the third node in the local reference system as (0,0,1), for the third node is located on the *Z'*-axis of the local reference system. The distance between the first node and the third node can be defined as 1 unit because the third node is only used to determine the direction of the three-dimensional frame cross-section. Matrix transformation will be introduced to determine the coordinates of the third node in the global reference. In the global reference system, suppose the coordinates of the first node N_1 are (x_1, y_1, z_1), the coordinates of the second node N_2 are (x_2, y_2, z_2).

The coordinate of the third node N_3 (x_3, y_3, z_3) can be obtained by moving the original point of the local reference system to the original point of the global reference system. After that, the local reference system was rotated around the *X*-axis by *α*, then the *Y*-axis by *β*, and finally around the *Z*-axis by *γ*. The angle *α* is between the x-axis of the local reference system and the x'-axis of the global reference system, *β* is between the y-axis of the local reference system and the y'-axis of the global reference system and *γ* is between the z-axis of the local reference system and the z'-axis of the global reference system.

Then, the vector rotation matrix in three-dimensional space is given by the product of the three rotation matrices:

$$\mathbf{r} = \mathbf{R}_{\boldsymbol{\alpha}}\mathbf{R}_{\beta}\mathbf{R}_{\gamma} \tag{60}$$

where *α*, *β*, and *γ* are respectively the rotation angles about *X*, *Y*, and *Z* axes.

And $\mathbf{R}_{\gamma}$, $\mathbf{R}_{\beta}$, $\mathbf{R}_{\alpha}$ are given by:

$$\mathbf{R}_{\boldsymbol{\gamma}} = \begin{bmatrix} cos\gamma & sin\gamma & 0 \\ -sin\gamma & cos\gamma & 0 \\ 0 & 0 & 1 \end{bmatrix} \tag{61}$$

$$\mathbf{R}_{\beta} = \begin{bmatrix} cos\beta & 0 & sin\beta \\ 0 & 1 & 0 \\ -sin\beta & 0 & cos\beta \end{bmatrix} \tag{62}$$

$$\mathbf{R}_{\alpha} = \begin{bmatrix} 1 & 0 & 0 \\ 0 & cos\alpha & -sin\alpha \\ 0 & sin\alpha & cos\alpha \end{bmatrix} \tag{63}$$

Then, the coordinate of N_3 in the global reference can be calculated:

$$N_3 = \boldsymbol{R}_{\boldsymbol{\alpha}}\boldsymbol{R}_{\beta}\boldsymbol{R}_{\gamma} n_3 + \mathrm{N1} \tag{64}$$

where n_3 is the coordinate of the third node in the local reference system, N_1 is the coordinate of the first node in the global reference system.

Since the stiffness matrix and mass matrix of each three-dimensional frame element are based on the local reference system, to assemble each three-dimensional frame element, a transformation matrix **T** will be proposed:

$$\mathbf{K}^{*} = \mathbf{T}^{\mathbf{T}}\mathbf{K}\mathbf{T} \tag{65}$$

$$\mathbf{M}^{*} = \mathbf{T}^{\mathbf{T}}\mathbf{M}\mathbf{T} \tag{66}$$

where **K**, **M** are the stiffness and mass matrices in the local reference system, **K*, M*** are the stiffness and mass matrices in the global reference system, **T** is the transformation matrix, and $\mathbf{T}^{\mathrm{T}}$ is the transpose matrix of **T**. The transformation matrix **T** is shown below:

$$\mathbf{T} = \begin{bmatrix} \mathbf{T_1} & 0 & 0 & 0 \\ 0 & \mathbf{T_1} & 0 & 0 \\ 0 & 0 & \mathbf{T_1} & \mathbf{0} \\ 0 & 0 & \mathbf{0} & \mathbf{T_1} \end{bmatrix} \tag{67}$$

$$\mathbf{T_1} = \begin{bmatrix} l_x & m_x & n_x \\ l_y & m_y & n_y \\ l_z & m_z & n_z \end{bmatrix} \tag{68}$$

where: $l_x, l_y, l_z, m_x, m_y, m_z, n_x, n_y, n_z$ are defined as:

$$\begin{aligned} l_x &= \vec{\mathrm{x}} \cdot \vec{\mathrm{X}}, \quad m_x = \vec{\mathrm{x}} \cdot \vec{\mathrm{Y}}, \quad n_x = \vec{\mathrm{x}} \cdot \vec{Z}, \\ l_z &= \vec{z} \cdot \vec{\mathrm{X}}, \quad m_y = \vec{z} \cdot \vec{\mathrm{Y}}, \quad n_y = \vec{z} \cdot \vec{\mathrm{Z}} \end{aligned} \tag{69}$$

$$\begin{aligned} l_y &= m_z n_x - n_z m_x \\ m_y &= n_z l_x - l_z n_x \\ n_y &= l_z m_x - m_z l_x \end{aligned} \tag{70}$$

where $\vec{\mathrm{x}}$, $\vec{y}, \vec{z}$ are the unit vectors in the X-axis, Y-axis and *Z*-axis in the local reference system, $\vec{\mathrm{X}}$, $\vec{\mathrm{Y}}$, $\vec{\mathrm{Z}}$ are the unit vectors in the X'-axis, Y'-axis and Z'-axis in the global reference system.

<u>3.4.2 Plane frame</u>

The plane frame shown in Figure 8 is constructed by welding three circular steel tubes together. Both ends of the frame are hinge-supported, and the frame has a particle mounted at point D at a distance *a* from point C. The frame is confined to undergo a planar motion which is modeled using beam elements with two translational degrees of freedom in the x- and y-directions and one rotational degree of freedom about the z-axis at a node. The height of the two even supports is h_1, or the lengths of line AC and line EG, the width of the plane frame is *w*, or the length of line CE, the radius of the tube is *r*, *E* and ρ the modulus of elasticity and density of the structure. The processes of determining density ρ, Young's modulus E, and the particle's mass installed on the plane frame are similar to that described in the beam section. A numerical example of plane frame structure is given in the following section.

Consider a one-floor plane frame structure as shown in Figure 8. A particle was mounted at point M 1m from point C. The lengths of line AC, line CE, and line EG are equal to 4 m, and the one-floor plane frame has a circular cross-section with radius r = 0.01 m, density ρ = 7870 kg/m^3 and Young's modulus E = 200 GPa. In addition, the one-floor plane frame structure is constrained within only in-plane vibration. The first natural frequency $\bar{\omega}_1$ is 2.7 Hz, and our goal is to determine the unknown mass *m* of the particle placed on the plane frame structure *m*. The initial guess for *m* is 20 kg. Through calculations, the unknown mass of the particle placed on the beam *m* was determined using Newton's method in only five iterations, and the result is shown in Table 6.

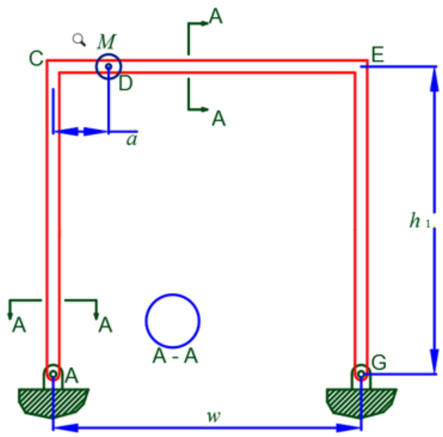

Figure 8. A plane frame structure with a point mass.

Table 6. The result of predicted mass, unit: kg for mass.

Mass Predicted	Actual Mass	Error
199.9	200	0.05%

3.4.3 Three-dimensional frame structure

Consider a three-dimensional frame structure as shown in Figure 9 with a circular cross-section with inner radius R_i, outer radius R_o, density ρ and Young's modulus E. The Three-dimensional frame system is supported rigidly at point A, and a particle m_1 is placed at a point on the line CD. The first natural frequency of the three-dimensional frame structure is $\bar{\omega}_1$. A numerical example is provided in the following section.

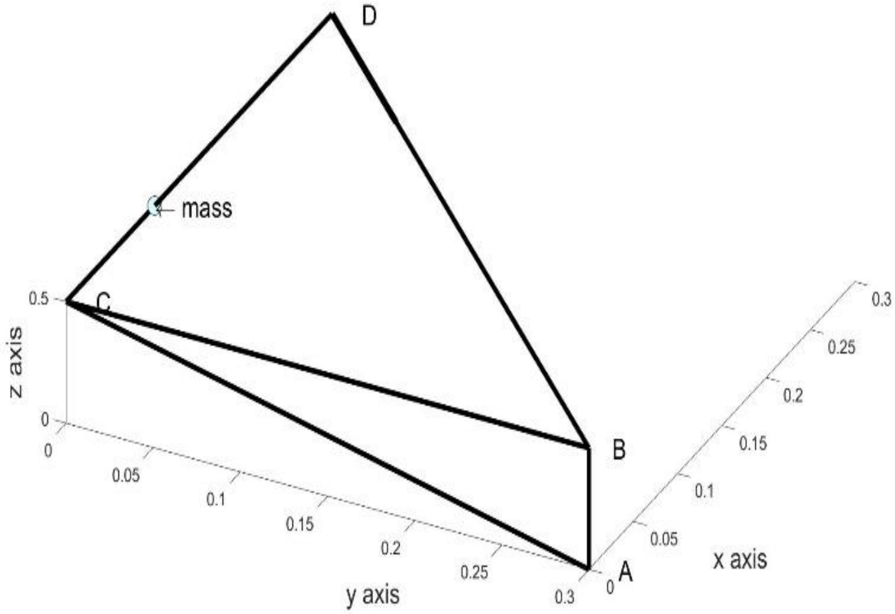

Figure 9. A three-dimensional frame

In a three-dimensional frame numerical example, the segments have lengths of AB=0.4 m, AC=0.5831 m, BC =0.2372 m, and BD= 0.3182 m and all have a circular cross-section with inner radius R_i=0.0035 m, outer radius R_o=0.005 m, density ρ = 7850 kg/m^3 and Young's modulus E = 200 GPa. Coordinates (unit:m) of the four points A, B, C, D are (0, 0.3, 0), (0, 0.3, 0.5), (0, 0, 0.5) and (0.3, 0, 0.5), respectively. This three-dimensional frame structure is fixed at point A, and a mass m_1 is placed 0.1458 m from point C. The first natural frequency $\overline{\omega}_1$ is 12.79Hz, and our goal is to determine the unknown mass of the particle placed on the Three-dimensional frame structure m_1. The initial guess for m_1 is 1 kg. Through calculations, and the result is shown in Table 7. The CPU time was 0.308s. To reduce the calculating time, component mode synthesis will be introduced in the following section.

Table 7. The result of predicted mass, unit: kg for mass.

Mass Predicted	Actual Mass	Error
10.7856	10.79	0.04%

3.4.3.1 Component mode synthesis

Component mode synthesis (CMS) solution techniques [23-24] are widely used in finite element analyses. It is effective for calculating the frequencies and mode shapes of complex structures such as airplanes and vehicles. The complete structure is considered an assemblage of the components, leading to an extensive finite element system. However, usually, only a few natural frequencies and corresponding mode shapes systems are needed. CMS can help to reduce the size of the matrix of the system and keep most of the detail. It is very effective for solving cases where the masses to be determined are located in a specific range. All the elements of a structure can be classified into CMS and normal finite elements. Elements on the component of the structure with no point mass were assigned to CMS, and others were assigned to the normal element. Then, by assembling the simplified stiffness matrix and mass matrix to calculate the natural frequency of the structure, not only an accurate result is obtained, but the calculation time of the CPU is also shortened.

One of the most popular substructure synthesis methods is the Craig-Bampton method [30]. There are two kinds of modes provided in the Craig-Bampton method: component mode and constrained mode. The component mode contains the vibration modes of individual substructures with the attachment degrees of freedom at nodes on lines or surfaces where substructures are connected or fixed. The component mode is the vibration mode of a single substructure with additional degrees of freedom, the degrees of freedom of the nodes specified on the lines or surfaces connected by the substructures. However, the constrained mode is a static displacement shape of a single substructure created by applying a unit displacement to each attached degree of freedom. Thus, all the attached degrees of freedom remain unchanged. Master degree of freedom refers to the degree of freedom that appears on the line or surface and is a dependent degree of freedom. The attached degree of freedom transforms the principal degree of freedom of a group or cluster into a super element.

To obtain the natural frequency of the structure, the eigenvalue problem of the equation can be derived as follows:

$$(-\omega_i^2[\mathbf{M}]_{\boldsymbol{CMS}} + [\mathbf{K}]_{\boldsymbol{CMS}})\{\mathbf{Z}\}_{\boldsymbol{i}} = \mathbf{0} \tag{71}$$

where i is a mode number, $[\mathbf{M}]_{\boldsymbol{CMS}}$ and $[\mathbf{K}]_{\boldsymbol{CMS}}$ are mass matrix and stiffness matrix of the synthesized structure, and $\{\mathbf{Z}\}_{\boldsymbol{i}}$ is a vector of amplitudes of component modes and attachment degree of freedoms.

By determining the attachment degrees of freedom of all substructures, the eigenvalue problem is solved as follows:

$$\left(-\omega_l^2[\mathbf{M}_{\boldsymbol{nn}}]_{\boldsymbol{j}} + [\mathbf{K}_{\boldsymbol{nn}}]_{\boldsymbol{j}}\right)\{\mathbf{D}_{\boldsymbol{l}}\}_{\boldsymbol{j}} = \mathbf{0} \tag{72}$$

$$[\boldsymbol{\Phi}]_{\boldsymbol{j}} = [\mathbf{D_1}\ \ \mathbf{D_2}\ \ \mathbf{D_3}\ \ \cdots \mathbf{D}_{\boldsymbol{k}}\ \ ]_{\boldsymbol{j}} \tag{73}$$

where n is a principal degree of freedom, l is a substructure mode, k is the number of modes retained in the mode matrix $[\boldsymbol{\phi}]_{\boldsymbol{j}}$, **M** and **K** are mass and stiffness matrices, and $\{\boldsymbol{D_l}\}_{\boldsymbol{j}}$ is a component amplitude vector.

The static analysis of the substructure stiffness matrix was given as follows:

$$\begin{bmatrix} \boldsymbol{K_{nn}} & \boldsymbol{K_{na}} \\ \boldsymbol{K_{na}^T} & \boldsymbol{K_{aa}} \end{bmatrix}_j \begin{bmatrix} \boldsymbol{\psi} \\ \boldsymbol{I} \end{bmatrix}_{\boldsymbol{j}} = \begin{bmatrix} \mathbf{0} \\ \mathbf{R} \end{bmatrix}_{\boldsymbol{j}} \tag{74}$$

where n is used to indicate master degrees of freedoms, a is attachment degrees of freedoms, $\boldsymbol{\psi}$ is the resulting vector of internal degrees of freedoms, **R** is the resultant vector of reactions at the attachment degrees of freedom. Solving for $\boldsymbol{\psi}$ yields:

$$[\boldsymbol{\psi}]_j = -[\mathbf{K}_{\boldsymbol{nn}}]_{\boldsymbol{j}}^{-\mathbf{1}}[\mathbf{K}_{\boldsymbol{na}}]_{\boldsymbol{j}} \tag{75}$$

The vector of amplitudes of the component $\{\mathbf{D}\}_{\boldsymbol{j}}$ can be represented as below:

$$\{\mathbf{D}\}_{\boldsymbol{j}} = \begin{Bmatrix} \mathbf{D}_{\boldsymbol{n}} \\ \mathbf{D}_{\boldsymbol{a}} \end{Bmatrix} = [\boldsymbol{W}]_{\boldsymbol{j}} \begin{Bmatrix} \mathbf{a} \\ \mathbf{D}_{\boldsymbol{a}} \end{Bmatrix} \tag{76}$$

where $\{\mathbf{a}\}_{\boldsymbol{j}}$ is a vector of modal coordinates analogous to $\{\mathbf{Z}\}$, and $[\mathbf{W}]_{\boldsymbol{j}}$ is a transformation matrix given as:

$$[\mathbf{W}]_{\boldsymbol{j}} = \begin{bmatrix} \boldsymbol{\phi} & \boldsymbol{\psi} \\ \mathbf{0} & \mathbf{I} \end{bmatrix}_j \tag{77}$$

For the j^{th} substructure, the reduced stiffness and mass matrices are:

$$\begin{aligned} [\mathbf{K}]_{\mathbf{CMS}} &= [\mathbf{W}]_{\boldsymbol{j}}^{\boldsymbol{T}}[\mathbf{K}]\,[\mathbf{W}]_{\boldsymbol{j}} \\ [\mathbf{M}]_{\mathbf{CMS}} &= [\mathbf{W}]_{\boldsymbol{j}}^{\boldsymbol{T}}[\mathbf{M}]\,[\mathbf{W}]_{\boldsymbol{j}} \end{aligned} \tag{78}$$

where **K** and **M** are the original stiffness and mass matrices. After the transformation was completed, the natural frequency was obtained according to the following equation:

$$\|[\mathbf{K}]_{\mathbf{CMS}} - \omega^2[\mathbf{M}]_{\mathbf{CMS}}\| = 0 \tag{79}$$

where ω is the natural frequency of the structure after the transformation.

When CMS was used to solve for the mass position shown in Figure 7, the line CE was assigned to the normal element because the mass was placed on it. However, the line AC and the line EG were assigned to CMS element. Thus, the CMS element will remain unchanged while the normal elements keep changing in each iteration. The normal elements and CMS elements were assembled to calculate each iteration's result until a satisfactory result was achieved.

3.4.3.2 Results of the example three-dimensional frame system

The solution solved by the MATLAB code using the traditional finite element method was 10.7856 kg which is the exact same as before and the CPU time was 0.308s. However, the result of using the CMS method is also 10.7856 kg, which is the same as that calculated using the traditional finite element method, and the CPU time is 1.02s, longer time than the traditional finite element method.

By comparing the two inverse techniques in this problem, the convergence time of the CMS method is usually shorter than that of the traditional inverse technique. Because the stiffness matrix and mass matrix of the line AB, line BD and line BC are calculated only once, but they were calculated in every iteration in the traditional method. However, the experimental results reveal a different outcome: the conventional inverse technique takes shorter than the CMS method. The CMS method calculation takes more time than the conventional finite element method in calculating line AB, line BD, and line BC in one iteration. In complex situations, using traditional techniques to calculate the stiffness matrix and mass matrix of the three-dimensional frame elements takes longer time than the calculation time of the CMS method.

3.5 Plate structure

A plate is a thin structural component that can be bent in two directions and has a specific thickness. The plate problem is widely used in structures that support lateral loads through bending [37]. There are many theories to solve different plate problems. One of the plate theories is the classic plate bending theory, known as Kirchhoff's plate theory [37]. The assumptions for the Kirchhoff plate theory are very similar to Euler-Bernoulli beam theory. One of the assumptions is that after the deformation, the straight line perpendicular to the midplane of the plate before the deformation remains the normal line, which also shows that the lateral deformation is ignored. Another popular theory is the Mindlin plate theory or first-order shear deformation theory. In this theory, the influence of the transverse shear deformation of the plate is taken into account. The Mindlin plate theory assumes that the straight line perpendicular to the undeformed middle plane of the plate remains straight but is not perpendicular to the deformed intermediate surface. In this dissertation, the plate element is derived based on Kirchhoff plate theory and Mindlin plate theory [37] that also includes the bending and transverse shear deformation. Each plate element has four nodes, and each node has three degrees of freedom which are respectively: u, the displacement in the z-direction; θ_x, the rotation of the x-axis; and θ_y, the rotation of the y axis as shown in Figure 10. And u, θ_x, and θ_y satisfy [46]:

$$u = \sum_{i=1}^{L_1} \sum_{j=1}^{L_2} N_i(\xi, \eta) H_j(\varsigma) u_{ij} \tag{80}$$

$$\theta_x = \sum_{i=1}^{L_1}\sum_{j=1}^{L_2} N_i(\xi,\eta)H_j(\varsigma)v_{ij} \tag{81}$$

$$\theta_y = \sum_{i=1}^{L_1} N_i(\xi,\eta)w_i \tag{82}$$

where L_1 and L_2 are the numbers of nodes in the xy-plane and the z-axis. For four-node quadrilateral shape functions, L_1=4 and L_2=2. $N_i(\xi,\eta)$ are shape functions used for the interpolation of the *xy*-plane, and $H_j(\varsigma)$ are shape functions used for the interpolation along the *z*-axis. And, u_{i1} and v_{i1} are displacements on the bottom surface; u_{i2} and v_{i2} are displacements on the top surface of the plate element.

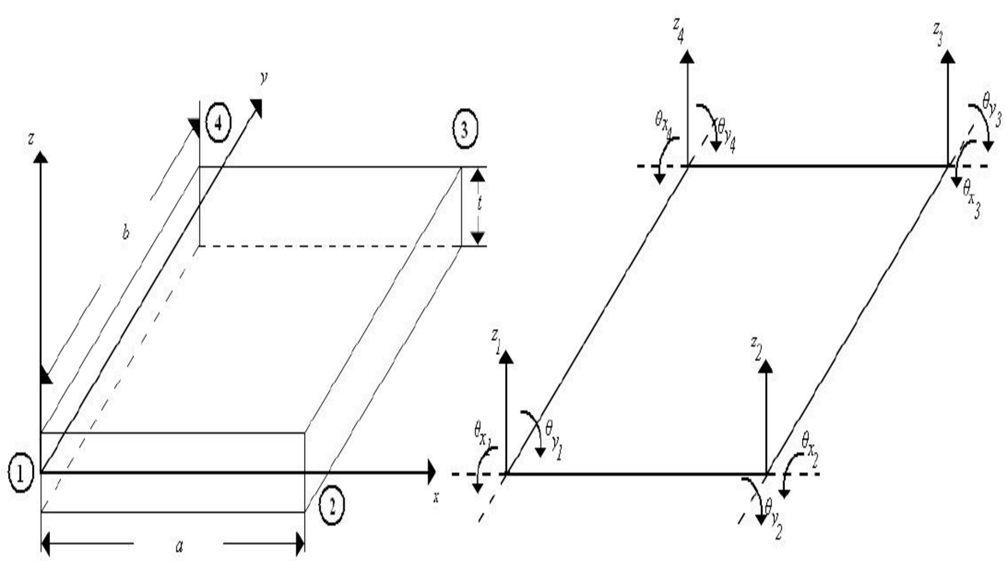

Figure 10. Degrees of freedom of a plate element [38].

The bending strain energy is:

$$U_b = \frac{1}{2}\int_{\Omega}\{{\sigma_b}^T\}\{\epsilon_b\}d\Omega \tag{83}$$

where σ_b is bending stress and $\epsilon_b$is bending strain, Ω is the plate domain. And bending strain ϵ_b can be expressed by the following equation [46]:

$$\{\epsilon_b\} = [\mathbf{B}_{\boldsymbol{b}}]\{d^e\} \tag{84}$$

$$[\mathbf{B}_{\mathrm{b}}] = [[B_{b1}]\ \ [B_{b2}]\ \ [B_{b3}]\ \ [B_{b4}]\,] \tag{85}$$

$$[\mathbf{B_{bi}}] = \begin{bmatrix} H_1\frac{\partial N_i}{\partial x} & 0 & H_2\frac{\partial N_i}{\partial x} & 0 & 0 \\ 0 & H_1\frac{\partial N_i}{\partial y} & 0 & H_2\frac{\partial N_i}{\partial y} & 0 \\ H_1\frac{\partial N_i}{\partial y} & H_1\frac{\partial N_i}{\partial x} & H_2\frac{\partial N_i}{\partial y} & H_2\frac{\partial N_i}{\partial x} & 0 \end{bmatrix} \tag{86}$$

$$\{\mathbf{d^e}\} = \{\{d_1^e\}\ \ \{d_2^e\}\,\{d_1^e\}\ \ \{d_2^e\}\}^T \tag{87}$$

$$\{\mathbf{d_i^e}\} = \{\, u_{i1}\ \ v_{i1}\ \ \ u_{i2}\ \ \ v_{i2}\ \ w_i\,\} \tag{88}$$

Bending stress σ_b can be expressed by the following equation [46]:

$$\{\sigma_b\} = [\mathbf{D_b}]\{\epsilon_b\} \tag{89}$$

where the material property matrix $\mathbf{D_b}$ is given as[46]:

$$[\mathbf{D_b}] = \frac{E}{1-\nu^2}\begin{bmatrix} 1 & \nu & 0 \\ \nu & 1 & 0 \\ 0 & 0 & \dfrac{1-\nu}{2} \end{bmatrix} \tag{90}$$

Here, E is Young's modulus, and ν is Poisson's ratio.
The stiffness matrix of a plate element for the bending part can be expressed:

$$[K_b^e] = \int_{\Omega^e} [B_b]^T [D_b][B_b] \, d\Omega^e \tag{91}$$

Transverse shear energy U_s:

$$U_s = \frac{1}{2}\int_{\Omega} \{\sigma_s{}^T\}\{\epsilon_s\} d\Omega \tag{92}$$

where σ_s is transverse shear stress, ϵ_s is transverse shear strain, Ω is the plate domain, and the transverse shear strain is ϵ_s:

$$\{\epsilon_s\} = [B_s]\{d^e\} \tag{93}$$

where

$$[B_s] = [[B_{s1}] \ [B_{s2}] \ [B_{s3}] \ [B_{s4}]] \tag{94}$$

$$[B_{si}] = \begin{bmatrix} N_i \frac{\partial H_1}{\partial z} & 0 & N_i \frac{\partial H_2}{\partial z} & 0 & \frac{\partial N_i}{\partial x} \\ 0 & N_i \frac{\partial H_1}{\partial z} & 0 & N_i \frac{\partial H_2}{\partial z} & \frac{\partial H_2}{\partial y} \end{bmatrix} \quad (95)$$

Transverse shear stress σ_s:

$$\{\sigma_s\} = [D_s]\{\epsilon_s\} \quad (96)$$

$$[D_s] = \frac{E}{2(1+\nu)} \begin{bmatrix} 1 & 0 \\ 0 & 1 \end{bmatrix} \quad (97)$$

The stiffness matrix of a plate element for the transverse shear part can be expressed:

$$[K_s^e] = \int_{\Omega^e} [B_s]^T [D_s][B_s] \, d\Omega^e \quad (98)$$

So the stiffness matrix of a plate element:

$$[K^e] = \int_{\Omega^e} [B_b]^T [D_b][B_b] \, d\Omega^e + \int_{\Omega^e} [B_s]^T [D_s][B_s] \, d\Omega^e \quad (99)$$

The mass matrix of a plate element:

$$[\mathbf{M}^e] = \int_{\Omega^e} [\mathbf{N}]^T [\mathbf{I}][\mathbf{N}] \; d\Omega^e \quad (100)$$

where **I** is the inertia matrix given by:

$$[\mathbf{I}] = \begin{bmatrix} \rho h & 0 & 0 \\ 0 & \dfrac{\rho h^3}{12} & 0 \\ 0 & 0 & \dfrac{\rho h^3}{12} \end{bmatrix} \tag{101}$$

where ρ is the density and h is the thickness.

3.5.1 A numerical example for a plate structure

Consider a plate structure as shown in Figure 11 with cross-section 30×1.85mm, the density of ρ = 7850 kg/m^3 and Young's modulus of 200 GPa. It is supported by both ends and other length parameters are marked in Figure 11. The first natural frequency $\bar{\omega}_1$ of the plate structure with the two point mass is 8.04 Hz. There are two particles mounted on the plate at point A and point B. The mass are, respectively, m_1 and 8g. Our goal is to determine the unknown mass of the particle placed on the plate structure m_1. The initial guess is 10g. Through calculations, the unknown mass of the particle placed on the plate m_1 was determined using Newton's, and the result is shown in Table 8.

Table 8. The result of predicted mass, unit: g for mass.

Mass predicted	Actual mass	Error
30.3	31	0.65%

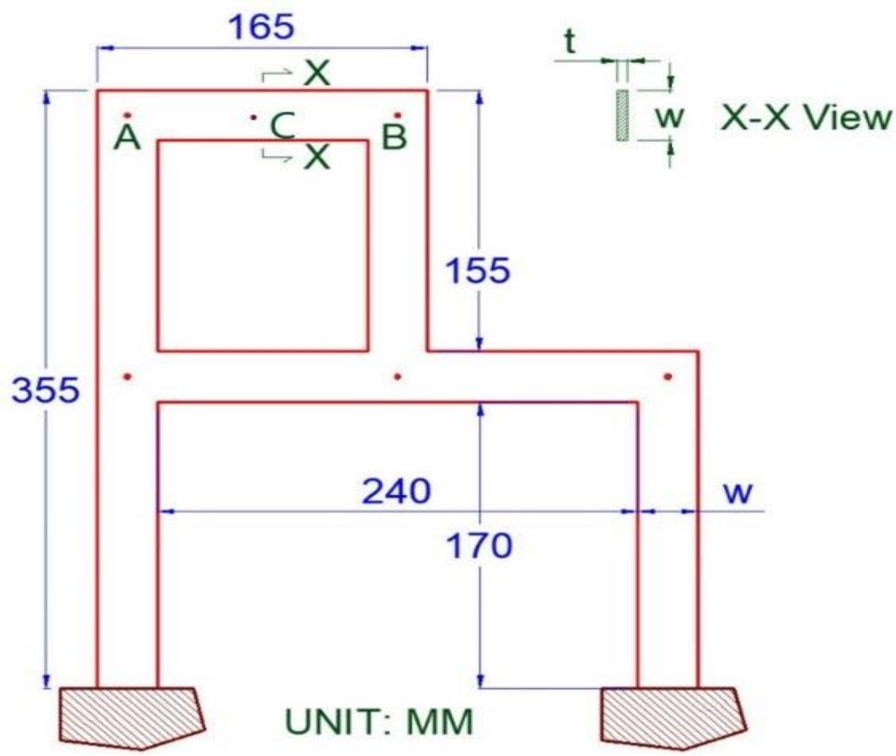

Figure 11. A plate frame.

CHAPTER FOUR

EXPERIMENTAL VERIFICATION

4.1 Introduction

This experiment aims to verify the accuracy of the inverse algorithm by comparing the theoretical and experimental value of the unknown particles that loaded on the specific place of a structure. The experimental values are the actual mass of the particles, while the theoretical values were calculated through an inverse algorithm using the measured natural frequencies, obtained by hammer impact test, of the structures loaded with particles. The tools and hardware used in this experiment, the theory of analyzing data, and the resulting data is described in the following section.

4.2 Data acquisition hardware

As shown in Figure 12, the experimental setup consists of a computer, data acquisition equipment, an impact hammer, an accelerometer, a steel beam, a clamp, and a mass. The computer is equipped with an Intel® Xeon® E-2176M processor (12M cache, up to 4.40 GHz) and 64 GB RAM, and is used to execute MATLAB code to collect and process data to obtain the natural frequencies of the beam. The impact hammer is used to strike the beam and record the force and time data. The data acquisition device is used to collect the acceleration data when the beam vibrates. Finally, the clamp is used to fix the beam to the table.

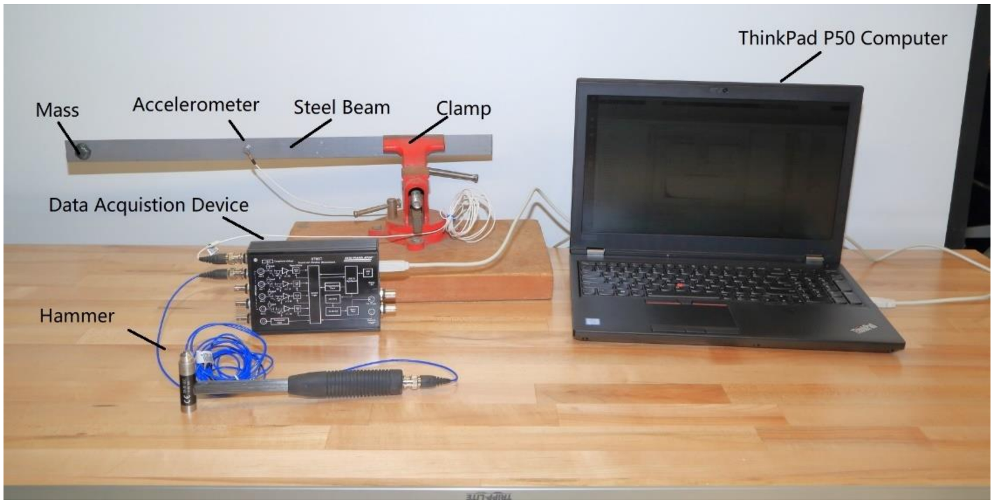

Figure 12. Experimental setup

4.3 Signal processing / FFT

Signal processing is a scientific technique that improves transmission, storage efficiency, and subjective quality and emphasizes or detects interest components in a measured signal. First, the data collection device obtains the time and acceleration data when the structure is excited into vibration. After that, the collected data is processed by filtering noise and detecting a range that the structure excited into vibration. Finally, Fast Fourier Transform (FFT) is used to process the data to capture the response signal's frequency.

Fourier transform (F.T.) is a mathematical transform that decomposes functions depending on space or time into functions depending on spatial or temporal frequency. It is widely used in sound processing, such as recording, compressing, equalizing, and image processing, such as color development and noise reduction [48]. Traditionally, the

Fourier transform of the function *f* is expressed by adding the circumflex $\hat{f}$, and is defined as:

$$\hat{f} = \int_{-\infty}^{\infty} f(x)\, e^{-2\pi i x \xi} dx \tag{102}$$

where ξ is a real number.

As shown in Figure 13 the signal curve consists of time and amplitude that obey Eqn. (103). Then, F.T. can be used for processing Eqn. (103) and the resulting curve is shown in Figure 14. From this curve, 20 and 300 Hz can be readily identified as domain frequencies identical to Eqn. (103) .

$$X = 5\, sin(40\pi t) + sin(600\pi t) \tag{103}$$

where *X* is the amplitude and *t* is the time of the signal.

The Fourier Transform (F.T.) is so powerful that natural frequencies can be obtained, even on signals with some noise. To test the effectiveness of F.T, a random noise was applied to a signal with an amplitude of 2 and corrupted by zero-mean random noise, as shown in Figure 15. Then, F.T. can be used for signals corrupted by zero-mean random noise, and the frequency curve can be drawn as shown in Figure 16. Nevertheless, it can still be identified that the natural frequencies are also 20 and 300Hz, identical to Eqn. (103).

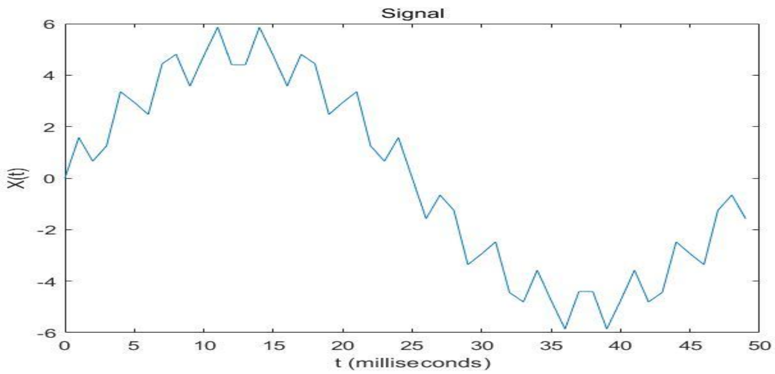

Figure 13. Signal

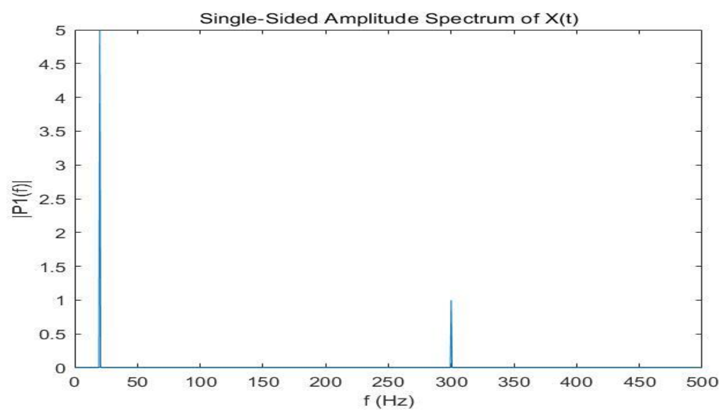

Figure 14. F.T. Curve

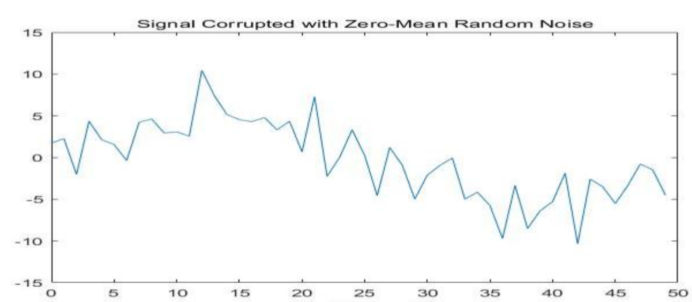

Figure 15. Signal Corrupted with Zero-Mean Random Noise

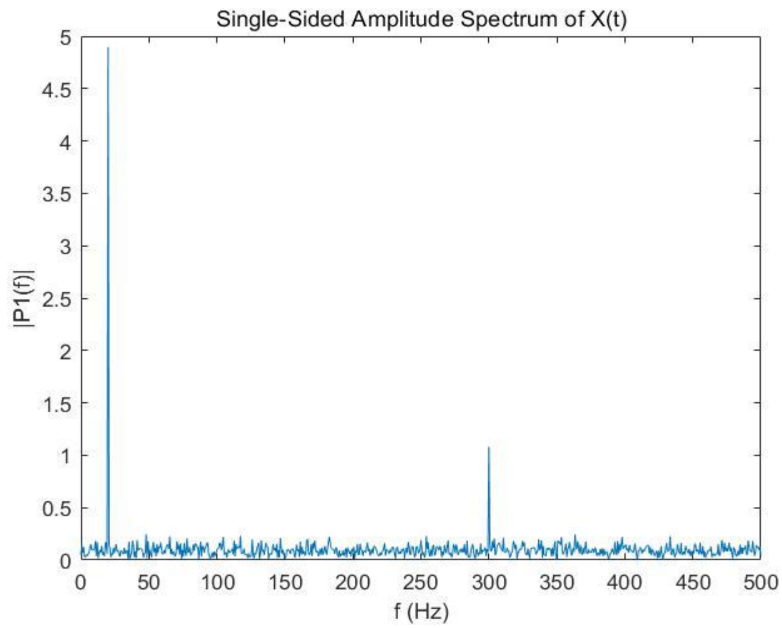

Figure 16. F.T. Curve of Signal Corrupted with Zero-Mean Random Noise

4.3.1 Fast Fourier Transform

A Fast Fourier Transform (FFT) is an algorithm that decomposes the Discrete Fourier Transform (DFT) matrix into sparse factor products and quickly calculates the frequency [64]. The FFT is useful in many fields such as engineering, science, mathematics, music, and image processing. Cooley and Tukey [49] first developed a modern FFT algorithm called the Cooley-Tukey algorithm, which proved to be faster than F.T. Following this, many researchers developed more FFT algorithms used under different conditions, such as Bruun's FFT algorithm, Rader's FFT algorithm, and hexagonal fast Fourier transform [49].

4.3.2 Signals Sampling Theorem

Signal sampling is the process of acquiring a discrete-time signal and converting it into a continuous-time signal. To analyze analog signals digitally, an analog-digital adapter or converter should be used. The sampling frequency of the analog-to-digital adapter plays an essential role in signal sampling. If the sampling frequency is too low, some information will be lost during the sampling process. However, if the sampling frequency is too high, overlapping areas will appear during the sampling period. Signals sampling theorem suggests a rule of a range of sampling frequency that is adequate to reduce the data loss of the transformation [50].

4.4 Hammer Impact Test

The hammer test is also called modal testing. It is a method to obtain the natural frequency, modal quality, modal damping ratio, and modal shape of the test structure by hitting the structure with a hammer [51]-[53].

4.4.1 Hammer Impact Test Process

To excite the structure, we impact it with a perfect impulse using the hammer. This will be a short period, which results in a constant amplitude in the frequency field. The duration of this time depends on the frequency content of the applied force. A particular hammer was used in the hammer impact test with a load cell at its tip to measure the impact force [57]. There is also a receiver and an analog-to-digital adapter for sampling data from the hammer and acceleration sensor. Then, after signal processing, the natural frequency of the test structure may be obtained.

4.4.2 Hammer Impact Test Using Different Tips

The hammer set provides five caps: soft impact cap, hard impact cap, medium impact cap, medium impact cap with formed tip cover, and super soft impact cap. The input force-frequency range can be controlled by changing the hammerhead in two ways: hammer mass and hammer stiffness. Increasing the weight of the hammerhead will result in a shorter contact time between the hammerhead and the structure. However, increasing the tip's stiffness will shorten the contact time between the hammer and the structure. Therefore, to obtain sufficient response data by impacting the hammer on the structure, an ultra-soft tip and a hammer with no increase in mass can be used to get a sufficiently long contact time between the hammer and the structure.

4.4.3 Accelerometer mounting

The technology of mounting the accelerometer to the vibrating structure between the measuring point and the sensor is crucial in obtaining accurate results. The method and type of installation affect the resonant frequency of the accelerometer. When this happens, the frequency range of the accelerometer will be affected. The most popular methods for mounting the accelerometer are Stud Mounting, Insulating Flange, Magnetic Base, Adhesive Pad, Direct Adhesive, Triaxial Mounting Cube, and Probe Mounting seen in Figure 17. Since the natural frequency of the determine structure is a comparably low frequency, it can be installed with Stud Mounting [55]-[56].

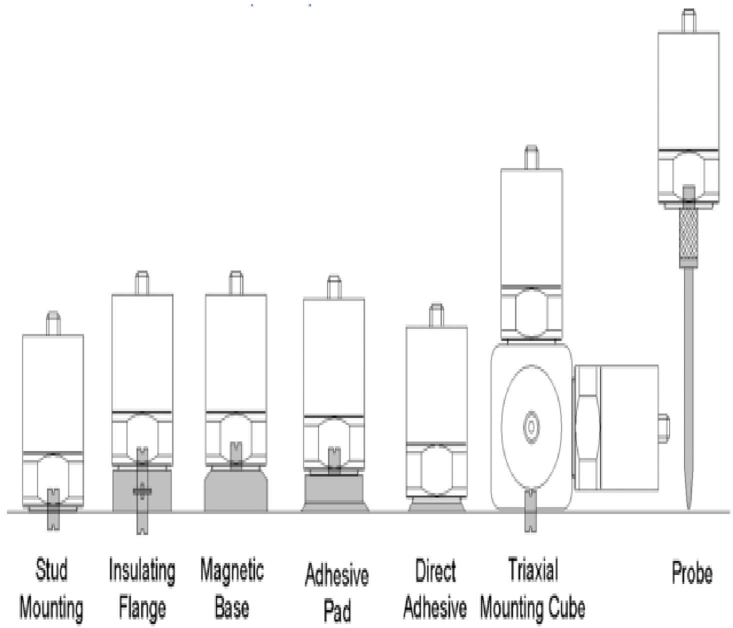

Figure 17. Methods of Accelerometer Mounting [54]

4.4.4 Data processing and analyzing

The acceleration response data was collected by the computer through the data acquisition device when the structure was excited and then stored and analyzed by the MATLAB codes using FFT to identify the natural frequencies.

4.5 Experimental validation of cantilever beam

To verify the inverse algorithm, we perform two sets of cantilever beam experiments. In the first set of experiments, we compared the experimental natural frequency measured by the hammer impact test and the theoretical one calculated by the beam theory. Then, we compared the predicted mass of particles calculated by the inverse algorithm and the actual one in the second. In the first set of experiments, 30 grams, 54 grams, and 78 grams of small particles were loaded to the position m_1 as shown in Figure 18; the acceleration sensor was placed at the position m_2. Then, the hammer impact test was performed five times for one condition to measure the natural frequencies of the entire system. However, in the second set of experiments, 30 grams, 54 grams, and 78 grams of small particles were loaded to the position m_2 as shown in Figure 18, the acceleration sensor was placed in the position m_1. Moreover, the hammer impact test was then used to measure the natural frequencies of the entire system. The length of the cantilever beam L = 0.45 m, cross-section $b \times h$= 31×1.34mm, density ρ = 7727kg/m^3 and Young's modulus of 210 GPa is used. The beam was fixed at one end and free at the other end, as shown in Figure 18.

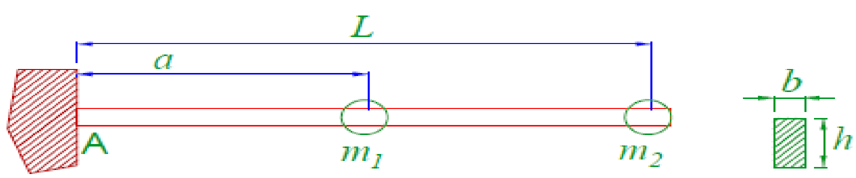

Figure 18. A Cantilever beam with a mass

4.5.1 Experimental validation result of a cantilever beam of group number one

Table 9. Results of experimental validation beam structure group #1, units: g for mass and Hz for natural frequencies.

Mass	Experimental ω_1	Theoretical ω_1	error
no mass	5.102	5.108	0
30	5.035	4.977	1%
54	4.976	4.850	3%
78	4.922	4.804	2%

As shown in Table 9, the experimental natural frequencies are the average value of the five repeated experimental results. Moreover, the results of predicted mass, based on experimental natural frequencies, are shown in Table 10. Unfortunately, the mass prediction error is large, which are 44%, 50%, and 39%, that is most likely because of the error of the experimental data used in predicting the mass of particles. Therefore, to verify the error is caused by the experimental data, we have carried out another set of mass predictions that regard the theoretical natural frequencies as the target of the natural frequency. The results are shown in Table 11, the errors in this set are small. If the mass of the particle is known, the position of sensor can also be determined by the reverse algorithm basing the experimental natural frequencies. Through calculations, the unknown position of the sensor placed on the beam m_1 was determined using Newton's method in 2 iterations shown in Table 12, the error in this set is small.

Table 10. First result of predicted mass group #1, unit: g for mass.

Mass Predicted	Actual Mass	Error
53.905	30	44%
108.08	54	50%
128.9	78	39%

Table 11. The second result of predicted mass group #1, unit: g for mass.

Mass Predicted	Actual Mass	Error
29.3	30	2%
54.5	54	1%
77	78	1%

Table 12. The result of predicted location of sensor group #1, unit: m for location for the particle.

Location Predicted	Actual Location	Error
0.43127	0.425	1%

4.5.2 Experimental Validation Beam Structure Group Number Two

As shown in Table 13, the experimental natural frequencies are the average value of the five repeated experimental results (second natural frequency, for the first natural frequency was missing in the FFT image). Moreover, the results of predicted mass, based on experimental natural frequencies, are shown in Table 14. The mass prediction error is large, which are 6%, 50%, and 39%, that is most likely because of the error of the experimental data used in predicting the mass of particles as mentioned in the above section. Therefore, to verify the error is caused by the experimental data, we have carried out another set of mass predictions that regard the theoretical natural frequencies as the target of the natural frequency. The results obtained are shown in Table 15, and the errors are small.

If the mass of the particle is known, the position of sensor can also be determined by the reverse algorithm basing the experimental natural frequencies. Through calculations, the unknown position of the sensor placed on the beam m_2 was determined using Newton's method in 2 iterations shown in Table 16.

Table 13. Results of experimental validation beam structure group #2 , units: g for mass and Hz for natural frequencies.

Mass	Experimental ω_1	Theoretical ω_1	error
no mass	33.696	33.354	1%
30	29.633	29.757	0.4%
54	28.136	28.744	2%
78	27.150	28.185	4%

Table 14. The first result of predicted mass group #2, unit: g for mass.

Mass Predicted	Actual Mass	Error
32	30	6%
80	54	33%
201	78	61%

Table 15. The second result of predicted mass group #2, unit: g for mass.

Mass Predicted	Actual Mass	Error
29.8	30	0.7%
53.9	54	0.2%
77.9	78	0.1%

Table 16. The result of predicted location of particle group #2, unit: m for location for the particle (the fixed end of the beam is the origin of the coordinate).

Location Predicted	Actual Location	Error
0.1843	0.17	8%

4.6 Experimental validation result of three-dimensional frame

In another experiment, we perform two sets of three-dimensional frame experiments as shown in Figure 19 and Figure 20. The first set focuses on the structure's natural frequency that compares the experimental natural frequency measured by the hammer impact test and the theoretical one calculated by the beam theory. The second set focuses on the particle's mass at the structure that compares the predicted mass of particles calculated by the inverse algorithm and the actual one. A sensor with 8g was placed in the point B. In the first group of experiments, particles weighing 31g and 81g were placed at point A. However, in the second group of experiments, particles weighing 31g and 81g were placed at point C, respectively. The cross-section is 30×1.85mm, the density of ρ = 7850 kg/m3 and Young's modulus of 200 Gpa, other parameters are marked in Figure 19.

4.6.1 Experimental Validation Three-Dimensional Frame Group Number One

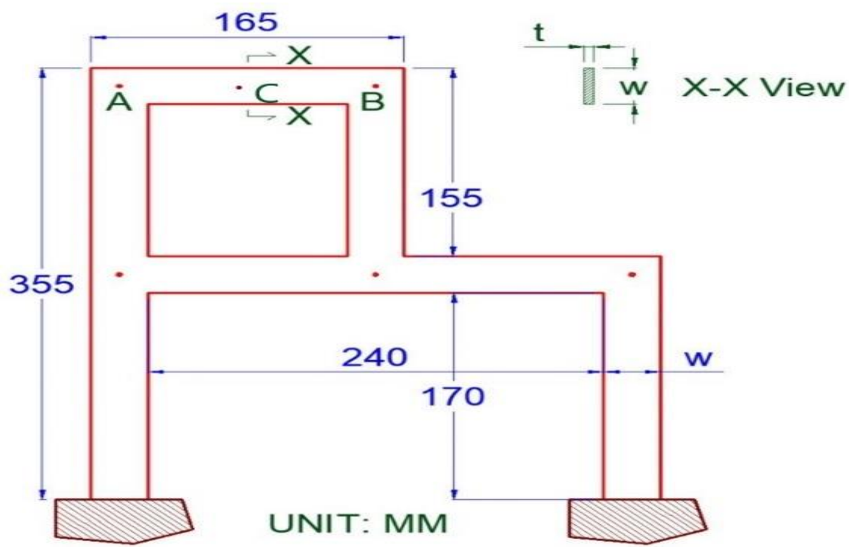

Figure 19. A plate frame with size labled.

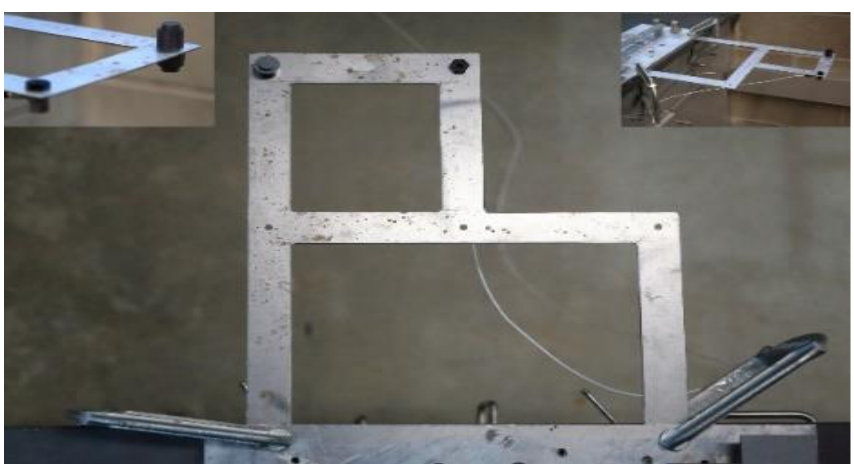

Figure 20. A plate frame.

Table 17. Results of experimental validation three-dimensional frame group #1 , units: g for mass and Hz for natural frequencies

Mass	Experimental ω_1	Theoretical ω_1	error
no mass	8.43	8.94	5.6%
31	7.71	8.16	5.6%
80	6.87	7.26	5.4%

The results of the natural frequencies are given in Table 17 for the five repeated hammer tests that were performed for each condition, and the average of the natural frequencies of the five tests are given.

As the results are shown in Table 17, the natural frequency errors of the first-order modes under the three conditions are not acceptable. This is because the boundary conditions are not fixed at both ends as assumed. To improve the accuracy of the algorithm, a different boundary condition is proposed. Two torsion rods are added at each end of the three-dimensional frame structure, as shown in Figure 21. To obtain the stiffness of the torsion rod at both ends of the three-dimensional frame structure, the GA algorithm was used to solve the inverse problem. After receiving the stiffness of the two torsion rods, the theoretical natural frequency of the three-dimensional frame structure is calculated again. Compared with the experimental natural frequencies, the results were presented in Table 18.

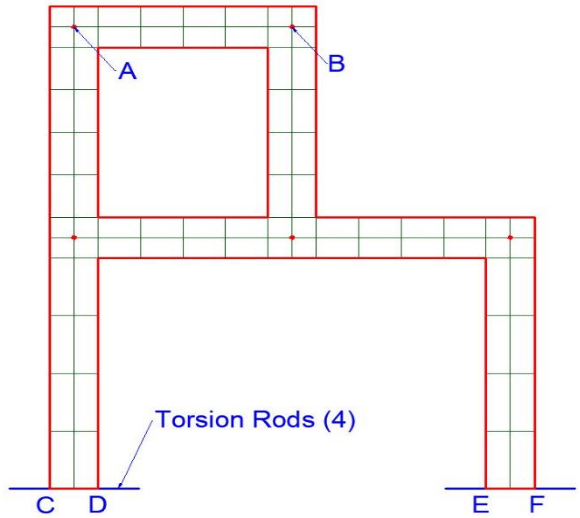

Figure 21. Finite element mesh for the plate frame with two point masses at A and B.

From Table 18, the first natural frequency error of the theoretical and experimental data of the three groups of conditions are all small. Then, the inverse algorithm was performed to predict the mass at a particular position using the target natural frequency that is the same as the first modal natural frequency of the experimental data. Finally, the results were presented in Table 19, the errors of the two predictions are all small.

Table 18. Second results of experimental validation three-dimensional frame group #1, units: g for mass and Hz for natural frequencies

Mass	Experimental ω_1	Theoretical ω_1	error
no mass	8.43	8.43	0.0%
31	7.71	7.70	0.1%
80	6.87	6.88	0.1%

Table 19. Results of predicted mass Group #1, unit: g for mass.

Mass Predicted	Actual Mass	Error
80.69	80	1%
31.284	31	1%

4.6.2 Experimental Validation Three-Dimensional Frame Group Number Two

The natural frequencies are given in Table 20 for the five repeated hammer tests that were performed for each condition, and the averages of the natural frequencies of the five tests are given.

Table 20.Results of experimental validation three-dimensional frame group #2, units: g for mass and Hz for natural frequencies

Mass	Experimental ω_1	Theoretical ω_1	error
no mass	8.43	8.43	0.0%
31	7.68	7.72	0.5%
80	6.90	6.88	0.2%

From Table 20, the first natural frequency error of the theoretical and experimental data of the three groups of conditions are all small. Then, using the target natural frequency that is the same as the first modal natural frequency of the experimental data, the inverse algorithm was performed to predict the quality at a particular position. The results are presented in Table 21, and the errors of the two predictions are small.

Table 21. Results of predicted mass Group #2, unit: g for mass.

Mass Predicted	Actual Mass	Error
78	80	3%
32	31	3%

4.7 Experimental validation result of the plate element

The final verification to verify the inverse algorithm is plate experiment. In the first set of experiments, we compared the experimental natural frequency measured by the hammer impact test and the theoretical one calculated by the plate theory. Then, we compared the predicted mass of particles calculated by the inverse algorithm and the actual one in the second. As shown in Figure 19, the plate structure has point A and point C where particles can be placed and one location point B where an accelerometer can be installed. There are two sets of experimental tests to verify the inverse algorithm: installing the particles at point A is the first group, at point C is the second group. In the first experiment set, an 8g acceleration sensor was installed at point B, and two different particles, 31g and 80g, were added to point A in turn. The hammer impact test was performed five times for one condition to measure the natural frequencies of the entire system in turn. Then, in the second set of experiments, the particles of 31g and 80g were placed in sequence at point C. After that, the hammer impact test was performed five times for one condition to measure the natural frequencies of the entire system in turn.

4.7.1 Experimental validation of plate structure group number one

The natural frequencies are given in Table 22 for the five repeated hammer tests that were performed for each condition, and the averages of the natural frequencies of the five tests are given.

Table 22. Results of experimental validation plate structure group #1, units: g for mass and Hz for natural frequencies

Mass	Experimental ω_1	Theoretical ω_1	error
no mass	8.43	8.84	4.6%
31	7.71	8.04	4.1%
80	6.87	7.11	3.4%

As shown in Table 22, the natural frequency errors of the first-order modes under the three conditions are not acceptable. This is because the boundary conditions are not fixed at both ends as assumed. To improve the accuracy of the algorithm, another boundary condition other than the fixed ends is proposed. First, two torsion rods are added at each end of the plate structure, as shown in Figure 21. Then, to obtain the stiffness of the torsion rods at both ends of the plate structure, the G.A. algorithm was used to solve the inverse problem. After receiving the stiffness of the two torsion rods, under the boundary conditions of adding two torsion rods at both ends, the theoretical natural frequency of the plate structure is calculated again. Compared with the experimental natural frequencies, the results were presented in Table 23.

Table 23. Second results of experimental validation plate structure group #1, units: g for mass and Hz for natural frequencies

Mass	Experimental ω_1	Theoretical ω_1	error
no mass	8.43	8.43	0.0%
31	7.71	7.68	0.4%
80	6.87	6.80	1.0%

In Table 23, the first mode natural frequency errors are all small. Then, the inverse algorithm was performed to predict the mass at a particular position using the target natural frequency that is the same as the first modal natural frequency of the experimental data. Finally, the results were presented in Table 24, and the errors of the two predictions are small.

Table 24. Results of predicted mass Group #1, unit: g for mass.

Mass Predicted	Actual mass	Error
75.87	80	5%
29.59	31	5%

4.7.2 Experimental validation of plate structure group number two

The natural frequencies are given in Table 25 for the five repeated hammer tests that were made for each condition, and the averages of the natural frequencies of the five tests are given.

Table 25. Results of experimental validation plate structure group #2, units: g for mass and Hz for natural frequencies

Mass	Experimental ω_1	Theoretical ω_1	error
no mass	8.43	8.43	0.0%
31	7.680	7.70	0.2%
80	6.90	6.85	0.7%

From Table 25, the first mode natural frequency error of the theoretical and experimental data of the three groups of conditions are all negligible. Then, using the target natural frequency that is the same as the first modal natural frequency of the experimental data, inversion was performed to predict the quality at a particular position. Finally, the results were presented in Table 26, the errors of the two predictions are small.

Table 26. Results of predicted mass Group #2, unit: g for mass.

Mass Predicted	Actual Mass	Error
76.63	80	3%
32.068	31	4%

CHAPTER FIVE

ATTRIBUTION

With the rapid development of computers, the finite element method has been able to provide a relatively accurate calculation of force, displacement, and natural frequency of complex objects. The actual natural frequency of the object reflects the real result of this microscopic effect. This has also become a practical and effective way for us to study the objects inside. In mechanical design, we always want to set a certain parameter of a part to the value we want, such as life, maximum stress, and natural frequency. Or in some detection experiments, one or several unknown parameters were found. So we are looking for an effective method to meet our requirements faster and more accurately. This is why we define our research as solution methodology for the constrained eigenvalue problem. In recent years, some people have developed some algorithms to solve such problems. But they still face some challenges or problems. For example, there is a difference between the model and the actual object, the stagnation in the solution, and the solution time is too long. These problems all affect the final solution speed and the accuracy of the results. Based on this, we optimized the theoretical mathematical model and proposed a calibrated theoretical model scheme. We have developed an algorithm that speeds up the solution time and reduces the solution stagnation rate. At the same time, we have made some adjustments to the ill-conditioned matrix generated in the solution, so that the program can continue to run. After these efforts, we established some models and solved some problems based on these models. To verify the reliability of the algorithm, we used Ansys to simulate and did some real experiments. The experimental models are beam structure, 3D-frame structure, and plate structure. The results of the experiment are satisfactory to us. We can use our algorithm to find out the weight of the mass loaded on the structure, the position of the mass loaded on the structure, the density of the object, and other parameters of the structure. To improve the accuracy, we also calibrated the theoretical model based on experimental data. The experiment proves that the calibration greatly improves the accuracy of the experimental results. In the future, we will apply this technology to more complex structures, and do more experiments and calibrations, so that this technology can be applied to complex structures.

CHAPTER SIX

CONCLUSIONS

In this dissertation, two numerical methods, Newton Raphson Iteration and Genetic Algorithm, were developed to determine the unknown parameters. The hammer impact test then help to validated the two numerical methods and their accuracies and convergence time. Compared with the Genetic Algorithm, the Newton-Raphson iterative method has the advantage of faster calculation but the disadvantage of not being able to generate a solution in some cases. Nevertheless, the two numerical methodologies can be used for applications such as discrete systems, beam problems, plane frames, three-dimensional frames, and plate problems. The first experimental verification was done using a cantilever beam through a hammer impact test to predict the particle's mass at the beam. Furthermore, the second experimental verification was done using a plate structure through a hammer impact test to predict the particle's mass at the plate. Each experiment was executed by five repeated times. The natural frequencies obtained by the hammer impact test for the five repeated times are similar and close to the theoretical natural frequencies, implying the experiment results are repeatable and accurate. However, when predicting the particle’s mass using the experimental natural frequencies, the predicted mass using the inverse algorithm Newton’s iteration or GA algorithm is not close to the actual mass. That is because a small error of the experimental natural frequencies is led to a big error of the predicted mass. To improve the accuracy of the predicted mass, we add a torsional bar to the structure and calculate the stiffness matrix of it using the inverse algorithm Newton’s iteration or GA algorithm. After the stiffness matrix of the torsional bar was obtained, we applied this to the boundary condition to the mathematical model. And the new predicted mass calculated by inverse algorithm basing on the developed mathematical model is very accurate compared with the actual mass.

In the future, the inverse algorithm will be developed for determining the unknown location parameter of the structure like beam, three-dimensional frame, and plate problems by applying the technique of moving finite element analysis [34]. This technique can help detect the small damage in some objects without destroying them or inspecting some buildings used for many years and determining the parameters of some unknown material like density, Young’s modulus, etc.

APPENDIX

The total mass and stiffness matrices of a 20-DOF spring-mass system:

$$\mathbf{M} = \begin{bmatrix} m_1 & 0 & 0 & & 0 & 0 & 0 \\ 0 & m_2 & 0 & \cdots & 0 & 0 & 0 \\ 0 & 0 & m_3 & & 0 & 0 & 0 \\ & \vdots & & \ddots & & \vdots & \\ 0 & 0 & 0 & & m_{n-2} & 0 & 0 \\ 0 & 0 & 0 & \cdots & 0 & m_{n-1} & 0 \\ 0 & 0 & 0 & & 0 & 0 & m_n \end{bmatrix} \tag{104}$$

$$\mathbf{K} = \begin{bmatrix} k_1+k_2 & -k_2 & 0 & 0 & & 0 & 0 & 0 & 0 \\ -k_2 & k_3+k_2 & -k_3 & 0 & \cdots & 0 & 0 & 0 & 0 \\ 0 & -k_3 & k_4+k_3 & -k_4 & & 0 & 0 & 0 & 0 \\ 0 & 0 & -k_4 & k_5+k_4 & & 0 & 0 & 0 & 0 \\ & \vdots & & & \ddots & & \vdots & & \\ 0 & 0 & 0 & 0 & & k_{n-2}+k_{n-3} & -k_{n-2} & 0 & 0 \\ 0 & 0 & 0 & 0 & \cdots & -k_{n-2} & k_{n-1}+k_{n-2} & -k_{n-1} & 0 \\ 0 & 0 & 0 & 0 & & 0 & -k_{n-1} & k_n+k_{n-1} & -k_n \\ 0 & 0 & 0 & 0 & & 0 & 0 & -k_n & k_n+k_{n+1} \end{bmatrix}$$

where $\overline{m}_1$ is an unknown mass.

The consistent mass matrix $\mathbf{M}^e$ and stiffness matrix $\mathbf{K}^e$ of an elementary beam element are given below [5].

$$\mathbf{M}^e = \frac{\rho A l}{420}\begin{bmatrix} 140 & 0 & 0 & 70 & 0 & 0 \\ 0 & 156 & 22l & 0 & 54 & -13l \\ 0 & 22l & 4l^2 & 0 & 13l & -3l^2 \\ 70 & 0 & 0 & 140 & 0 & 0 \\ 0 & 54 & 13l & 0 & 156 & -22l \\ 0 & -13l & -3l^2 & 0 & -22l & 4l^2 \end{bmatrix} \tag{105}$$

$$
\mathbf{K}^{\mathrm{e}} = \begin{bmatrix}
\frac{\mathrm{A.E.}}{l} & 0 & 0 & \frac{-\mathrm{A.E.}}{l} & 0 & 0 \\
0 & \frac{12\mathrm{EI}}{l^3} & \frac{6\mathrm{EI}}{l^2} & 0 & \frac{-12\mathrm{EI}}{l^3} & \frac{6\mathrm{EI}}{l^2} \\
0 & \frac{6\mathrm{EI}}{l^2} & \frac{4\mathrm{EI}}{l} & 0 & \frac{-6\mathrm{EI}}{l^2} & \frac{2\mathrm{EI}}{l} \\
\frac{-\mathrm{A.E.}}{l} & 0 & 0 & \frac{\mathrm{A.E.}}{l} & 0 & 0 \\
0 & \frac{-12\mathrm{EI}}{l^3} & \frac{-6\mathrm{EI}}{l^2} & 0 & \frac{12\mathrm{EI}}{l^3} & \frac{-6\mathrm{EI}}{l^2} \\
0 & \frac{6\mathrm{EI}}{l^2} & \frac{2\mathrm{EI}}{l} & 0 & \frac{-6\mathrm{EI}}{l^2} & \frac{4\mathrm{EI}}{l}
\end{bmatrix} \tag{106}
$$

where ρ is the density of the beam, l the length of the beam element, A the cross-section area, I moment of inertia of the cross-section, and Young's modulus of the material.

The consistent mass matrix $\mathbf{M}^{\mathrm{e}}$ and stiffness matrix $\mathbf{K}^{\mathrm{e}}$ of a three-dimensional frame element are given [47].

$$
\mathbf{M}^{\mathrm{e}} = \frac{\rho A l}{210}\begin{bmatrix}
70 & 0 & 0 & 0 & 0 & 0 & 35 & 0 & 0 & 0 & 0 & 0 \\
 & 78 & 0 & 0 & 0 & 22\mathrm{a} & 0 & 27 & 0 & 0 & 0 & -13a \\
 & & 78 & 0 & -22\mathrm{a} & 0 & 0 & 0 & 27 & 0 & 13a & 0 \\
 & & & \frac{70\mathrm{I}_{x\prime}}{A} & 0 & 0 & 0 & 0 & 0 & \frac{-35\mathrm{I}_{x\prime}}{A} & 0 & 0 \\
 & & & & 8a^2 & 0 & 0 & 0 & -13\mathrm{a} & 0 & -6a^2 & 0 \\
 & & & & & 8a^2 & 0 & 13\mathrm{a} & 0 & 0 & 0 & -6a^2 \\
 & & & & & & 70 & 0 & 0 & 0 & 0 & 0 \\
 & & & & & & & 78 & 0 & 0 & 0 & -22\mathrm{a} \\
 & & & & & & & & 78 & 0 & 22\mathrm{a} & 0 \\
 & & & sy. & & & & & & \frac{70\mathrm{I}_{x\prime}}{A} & 0 & 0 \\
 & & & & & & & & & & 8a^2 & 0 \\
 & & & & & & & & & & & 8a^2
\end{bmatrix} \tag{107}
$$

$$\mathbf{K}^{\mathrm{e}} =$$

$$\begin{bmatrix}
\frac{\mathrm{A.E.}}{l} & 0 & 0 & 0 & 0 & 0 & -\frac{\mathrm{A.E.}}{l} & 0 & 0 & 0 & 0 & 0 \\
 & \frac{12\mathrm{EI}_{z'}}{l^3} & 0 & 0 & 0 & \frac{6\mathrm{EI}_{z'}}{l^2} & 0 & -\frac{12\mathrm{EI}_{z'}}{l^3} & 0 & 0 & 0 & \frac{6\mathrm{EI}_{z'}}{l^2} \\
 & & \frac{12\mathrm{EI}_{y'}}{l^3} & 0 & -\frac{6\mathrm{EI}_{y'}}{l^2} & 0 & 0 & 0 & -\frac{12\mathrm{EI}_{y'}}{l^3} & 0 & -\frac{6\mathrm{EI}_{y'}}{l^2} & 0 \\
 & & & \frac{\mathrm{GJ}}{l} & 0 & 0 & 0 & 0 & 0 & -\frac{\mathrm{GJ}}{l} & 0 & 0 \\
 & & & & \frac{4\mathrm{EI}_{y'}}{l} & 0 & 0 & 0 & \frac{6\mathrm{EI}_{y'}}{l^2} & 0 & \frac{2\mathrm{EI}_{y'}}{l} & 0 \\
 & & & & & \frac{4\mathrm{EI}_{z'}}{l} & 0 & -\frac{6\mathrm{EI}_{z'}}{l^2} & 0 & 0 & 0 & \frac{2\mathrm{EI}_{y'}}{l} \\
 & & & & & & \frac{\mathrm{A.E.}}{l} & 0 & 0 & 0 & 0 & 0 \\
 & & & & & & & \frac{12\mathrm{EI}_{z'}}{l^3} & 0 & 0 & 0 & -\frac{6\mathrm{EI}_{z'}}{l^2} \\
 & & & & & & & & \frac{12\mathrm{EI}_{y'}}{l^3} & 0 & \frac{6\mathrm{EI}_{y'}}{l^2} & 0 \\
 & & sy. & & & & & & & \frac{\mathrm{GJ}}{l} & 0 & 0 \\
 & & & & & & & & & & \frac{4\mathrm{EI}_{y'}}{l} & 0 \\
 & & & & & & & & & & & \frac{4\mathrm{EI}_{z'}}{l}
\end{bmatrix}$$

where ρ is the density of the beam, l the length of the beam element, A the cross-section area, $I_{x'}$ moment of inertia of the cross-section around X'-X' axis at T, $I_{z'}$ moment of inertia of the cross-section around Z'-Z' axis at T, $I_{Y'}$ moment of inertia of the cross-section around Y'-Y' axis at T, $I_{Y'}$, $I_{y'z'}$ moment of inertia of the cross-section around Y'-Y'and Z'-Z' axes at T, J polar moment of inertia, G shear modulus of the material, and Young's modulus of the material.

REFERENCES

1 J. Ormondroyd and J.P. Den Hartog, "The theory of the dynamic vibration absorber. ",Transactions of ASME, 50(APM-50-7), 9–22, 1928

2 Vonflotow, A., Beard, A.R., & Bailey, D.C. (1994). "Adaptive tuned vibration absorbers: Tuning laws, tracking agility, sizing, and physical implementations. ", New Civil Engineer, 437-454.

3 Brennan, M.. "Vibration control using a tunable vibration neutralizer." Proceedings of the Institution of Mechanical Engineers, Part C: Journal of Mechanical Engineering Science 211 (1997): 108 - 91.

4 Gander W., Golub G.H., von Matt U., 1989, "A constrained eigenvalue problem. Linear Algebra and its Applications", Volumes 114–115, 815-839

5 Azizi, A., Dourali, L., Zareie, S., & Rad, F.P. (2009). "Mathematical Modeling of Deflection of a Beam: A Finite Element Approach. 2009 Second International", Conference on Environmental and Computer Science, 161-164.

6 Bhardwaj M, Pierson K, Reese G, Walsh T, Day D, Alvin K, Peery J, Farhat C, Lesoinne M. Salinas: "a scalable software for high-performance structural and solid mechanics simulations. ", Proceedings of the IEEE/ACM SC2002 Conference, Baltimore, Maryland, 2002.

7 Lehoucq, R., Sorensen, D., & Yang, C. (1998). "ARPACK users' guide - solution of large-scale eigenvalue problems with implicitly restarted Arnoldi methods. ", Software, environments, tools.

1. Maschhoff, K. and D. Sorensen. "P_ARPACK: An Efficient Portable Large Scale Eigenvalue Package for Distributed Memory Parallel Architectures." PARA (1996).
2. Baker C G., Lehoucq R.B., "Constrained Eigenvalue Problems", CSRI Summer Proceedings, (2007) 68-72.
3. Ram, Y. "A Constrained Eigenvalue problem and nodal and modal control of vibrating systems." Proceedings of the Royal Society A: Mathematical, Physical and Engineering Sciences 466 (2009): 831 - 851.
4. Gu, W., Ma, T., Shen, L., Li, M., Zhang, Y., & Zhang, W. (2019). " Coupled electrical-thermal modelling of photovoltaic modules under dynamic conditions. ", Energy, 188, 116043.
5. Wang, J., Zhaijun, L., Zhong, M., Wang, T., Sun, C., & Li, H. (2019). "Coupled thermal–structural analysis and multi-objective optimization of a cutting-type energy-absorbing structure for subway vehicles. ", Thin-walled Structures, 141, 360-373.
6. Mises, R. and H. Pollaczek-Geiringer. “Praktische Verfahren der Gleichungsauflösung .” Zamm-zeitschrift Fur Angewandte Mathematik Und Mechanik 9: 152-164.
7. Pohlhausen, E.. “Berechnung der Eigenschwingungen statisch-bestimmter Fachwerke.” Zamm-zeitschrift Fur Angewandte Mathematik Und Mechanik 1: 28-42.
8. Rainer Kress, "Numerical Analysis," Springer, 1991. ISBN 0-387-98408-9

9. John. G. F. Francis, " The QR Transformation A , unitary Analogue to the L.R. Transformation—Part 1", The Computer Journal, Volume 4, Issue 3, 1961, Pages 265–271.

10. Press, W., Flannery, B., Teukolsky, S., Vetterling, W., & Gould, H. (1987). "Numerical Recipes", The Art of Scientific Computing. American Journal of Physics, 55, 90-91.

11. Cuppen, J.. “A divide and conquer method for the symmetric tridiagonal eigenproblem.” Numerische Mathematik 36 (1980): 177-195.

12. Claude, B., Duigou, L., Girault, G., & Cadou, J. (2017). "Eigensolutions to a vibroacoustic interior coupled problem with a perturbation method. ", Comptes Rendus Mecanique, 345, 130-136.

13. Chapra, S. and R. P. Canale. "Numerical Methods for Engineers." (1986).

14. Abadie. J & J. Carpentier, "Generalization of the Wolfe reduced gradient method to the case of nonlinear constraints", in Optimization, (R. Fletcher, Ed.), Academic Press, New York, 1969.

15. Press WH, Flannery BP, Teukolsky SA, and Vetterling WT, "Numerical Recipes: The Art of Scientific Computing", New York: Cambridge University Press, 1996.

16. Golub, G. and C. Loan. "Matrix computations (3rd ed.)." , Johns Hopkins University Press,1996.

17. Abdullah Konak, David W. Coit, Alice E. Smith, "Multi-objective Optimization using genetic algorithms: A tutorial", Reliability Engineering & System Safety, Volume 91, Issue 9,2006, Pages 992-1007, ISSN 0951-8320.

18. Reeves, C. and J. Rowe. "Genetic Algorithms—Principles and Perspectives." Operations Research/Computer Science Interfaces Series (2002).

19. Chien, C., Huang, Y., & Hu, C. (2009). "A hybrid approach of data mining and genetic algorithms for rehabilitation scheduling. ", Int. J. Manuf. Technol. Manag., 16, 76-100.

20. Horn, R. and Charles R. Johnson. "Matrix analysis.", Cambridge University Press,1985.

21. Reklaitis GV, Ravindran A, and Ragsdell KM, "Engineering Optimization: Methods and Applications," New York: John Wiley, 1983.

22. Kindova-Petrova, Dimitrina. "Vibration-Based Methods For Detecting A Crack In A Simply Supported Beam." Journal of Theoretical and Applied Mechanics 44 (2014): 69 - 82.

23. Zissimos P. Mourelatos, Dimitris Angelis and John Skarakis (October 2nd 2012). "Vibration and Optimization Analysis of Large-Scale Structures using Reduced-Order Models and Reanalysis Methods", Advances in Vibration Engineering and Structural Dynamics, Francisco Beltran-Carbajal, IntechOpen, DOI: 10.5772/51402.

24. Baker, C. and R. Lehoucq. "Preconditioning constrained eigenvalue problems." Linear Algebra and its Applications 431 (2009): 396-408.

25. Xu, Q. and J. Prozzi. "A finite-element and Newton-Raphson method for inverse computing multilayer moduli." Finite Elements in Analysis and Design 81 (2014): 57-68.

26. Meirovitch, L. and H. Saunders. "Computational Methods in Structural Dynamics." Journal of Vibration and Acoustics-transactions of The Asme 106 (1980): 4-5.

27. Gao, F. and W. Sun. "Nonlinear finite element modeling and vibration analysis of the blisk deposited strain-dependent hard coating." Mechanical Systems and Signal Processing 121 (2019): 124-143.

28. Beer, F. (1981). "Mechanics of materials / Ferdinand P. Beer, E. ", Russell Johnston, JR., John T. Dewolf.

29. Qu, Z. "Model Order Reduction Techniques with Applications in Finite Element Analysis." , Springer-Verlag London ,2004.

30. Craig, R. and S. Benzley. "Structural Dynamics: An Introduction to Computer Methods." , John Wiley and Sons Ltd, 1981.

31. R. R. Craig Jr., "A Review of Time-Domain and Frequency-Domain Component-Mode Synthesis Methods," Int. J. of Analytical and Experimental Modal Analysis, Vol. 2, No. 2, 1987, pp. 57-72.

32. Miller, K. & Miller, R., "Moving finite elements I. SIAM Journal Numerical Analysis", 18(6), pp. 1019–1032, 1981.

33. Miller, K., "Moving finite elements II. SIAM Journal Numerical Analysis", 18(6), pp.1033–1057, 1981.

34. Gu, Randy J. “Moving finite element analysis for the identification of elastic beams.” Finite Elements in Analysis and Design 4 (1988): 267-278.

35. L. Meirovitch and M. K. Kwak, "Rayleigh-Ritz Based Substructure Synthesis for Flexible Multibody Systems," AIAA Journal, Vol. 29, No. 10, 1991, pp. 1709-1719.

36. Cook, R., Malkus, D., Plesha, M., & Witt, R. "Concepts and Applications of Finite Element Analysis",Wiley, 2001.

37. Bathe, K. "Finite Element Procedures." , Klaus-Jurgen Bathe, 1995.

38. Melo, G.P., Fernandes, F.V., Koroishi, E.H., & Fernandes, V. (2011). "DIAGNOSIS OF FAULT USING STATE OBSERVERS IN SYSTEMS WITH DYNAMIC VIBRATIONS ABSORBERS (DVAs) ".

39. K-J. Bathe and E. N. Dvorkin, "Mindlin/Reissner Plate Theory and A Mixed Interpolation A Four-Node Plate Bending Element", International Journal for Numerical Methods in Engineering, Vol. 21, 367-383 (1985).

40. A. J. M. Ferreira, " MATLAB codes for finite element analysis of solids and structures", Springer Science, 2009.

41. G. C. Archer, T. M. Whalen, "Development of rotationally consistent diagonal mass matrices for plate and beam elements", Comput. Methods Appl. Mech. Engrg., 194 (2005) 675–689.

42. E. Hinton, T. Rock, O.C. Zienkiewicz, "A note on mass lumping and related processes in the finite element method, Earthq. Engrg. Struct. Dyn. 4 (3) (1976) 245–249.

43. Julius S. Bendat, Allan G. Piersol, "Random Data: Analysis and Measurement Procedures", Wiley, 2011.

44. Brüel & Kjær, "Frequency Analysis – Handbook ", 3rd edn., 1987.

45. P. Avitabile, "Modal Testing: A Practitioner's Guide", Wiley, 2017.

46. Kwon, Young W., and H. Bang. "The finite element method using MATLAB (2nd ed.)." , CRC Press, 2000.

47. Lopez, R. D. "A three-dimensional Finite Beam Element for the Modelling of Composite Wind Turbine Wings." 2013.

48. Bracewell, R. N. "The Fourier Transform and Its Applications (3rd ed.)." , McGraw-Hill Science, 2000.

49. Heideman, M., Johnson, D., & Burrus, C. (1984). "Gauss and the history of the fast fourier transform. ", IEEE ASSP Magazine, 1, 14-21.

50. Shannon, C.. "Communication in the presence of noise." Proceedings of the IEEE 72 (1984): 1192-1201.

51. Castellini, P., Revel, G.M., & Scalise, L. (2004). "Measurement of vibrational modal parameters using laser pulse excitation techniques. ", Measurement, 35, 163-179.

52. Wilson, John S. "Sensor Technology Handbook.", Newnes, 2004.

53. Ahn, S., Jeong, W., & Yoo, W. (2005). " Improvement of impulse response spectrum and its application. Journal of Sound and Vibration", 288, 1223-1239.

54. Innomic company

55. David A. Corelli. "How sensor mounting significantly affects vibration measurements.".

56. Dumont, M., Cook, A., & Kinsley, N. "Acceleration Measurement Optimization: Mounting Considerations and Sensor Mass Effect", Springer, 2016.

57. Roy, P. K. and N. Ganesan. "Transient response of a cantilever beam subjected to an impulse load." Journal of Sound and Vibration 183 (1995): 873-880.

58. Roth S., Neumeister P., Semenov A.S., Balke H. (2011) "Finite Element Simulation of the Non-remanent Straining Ferroelectric Material Behaviour Based on the Electrostatic Scalar Potential:Convergence and Stability." ,In: Kuna M., Ricoeur A. (eds) IUTAM Symposium on Multiscale Modelling of Fatigue, Damage and Fracture in Smart Materials. IUTAM Bookseries, vol 24. Springer, Dordrecht.

59. George B. Dantzig. "The Nature of Mathematical Programming." Mathematical Programming Glossary, INFORMS Computing Society.

60. Ma, F., Imam, A., & Morzfeld, M. (2009). "The decoupling of damped linear systems in oscillatory free vibration. ", Journal of Sound and Vibration, 324, 408-428.

61. Schwarzenberg-Czerny, A.. "On matrix factorization and efficient least-squares solution." Astronomy & Astrophysics Supplement Series 110 (1995): 405.

62. Magnus, J. and H. Neudecker. "Matrix Differential Calculus with Applications in Statistics and Econometrics.",Wiley, 1988.

63. Bunch, J. and J. Hopcroft. "Triangular Factorization and Inversion by Fast Matrix Multiplication." Mathematics of Computation 28 (1974): 231-236.

64. Loan, C.. "Computational Frameworks for the Fast Fourier Transform.", Society for Industrial and Applied Mathematics, 1992.

65. Nemirovsky, J. and E. Shimron. "Utilizing Bochner's Theorem for Constrained Evaluation of Missing Fourier Data." arXiv: Medical Physics, 2015.